UNIVERSITY OF CALIFORNIA SAN DIEGO

Positional cloning and characterization of the *Rotten Ear* (*Rte*) gene in *Zea mays*

A Thesis submitted in partial satisfaction of the requirements
For the degree Master of Science

in

Biology

by

Ma Zara Emilia Marañon Tabi

Committee in charge:

Professor Robert Schmidt, Chair
Professor Nigel Crawford
Professor Martin Yanofsky

2012

The Thesis of Ma Zara Emilia Marañon Tabi is approved and is acceptable in quality and form for publication on microfilm and electronically:

Chair

University of California, San Diego

2012

DEDICATION

I dedicate this thesis to my big little brother Patrick, for his emotional (and monetary!) support during the latter half of my UCSD career. This would have been very difficult without you. Thank you.

TABLE OF CONTENTS

ACKNOWLEDGEMENTS

There are so many people to thank! First and foremost I would like to express my appreciation to Dr. Robert Schmidt for giving me the opportunity to work in his lab as an BS/MS student, allowing me to apply the lessons I've learned here at UCSD to actual research, and giving me this extra time to figure out what I really wanted to do. I understand his moments with us at the Schmidt Lab were very limited for the latter half of this thesis project and I am very grateful for what advice and insight he was able to provide as the chair of my committee.

A thousand thanks to the wonderful Dr. Nigel Crawford and Dr. Marty Yanofsky, for not only agreeing to be part of my thesis committee, but for taking time out of their busy schedules to answer any and all of my questions about my project, photography, medicine, and life as we know it.

I would also like to thank the members of the Yanofsky lab, for their friendship and humor, but especially for saving my sanity and keeping me in good spirits during this inarguably challenging chapter in my life. I am truly grateful.

And finally, many thanks to Andrea Gallavotti for his stern guidance and for teaching me all the lab techniques and scientific concepts I needed for the successful completion of this thesis. I would also like to thank the current and former members of the Schmidt lab, for all of their support and insight they gave throughout my time here, for the numerous happy hours and lab meetings, and for making lab like a second home to me.

Figures 1 and 2 were provided by committee chair Dr. Robert Schmidt and previously published in "Development of the Inflorescences" by Vollbrecht, E., and Schmidt, R. (2009). This chapter can be found in Handbook of Maize: It's Biology, Bennetzen, Jeff L., and Hake, Sarah C. eds., (New York, New York: Springer) pp. 13-40.

I would like to acknowledge the work of Michael Muszynski of Iowa state University, who not only provided us with SEM imagery of the young ear primordium, but additional *rotten ear* alleles as well. I would also like to acknowledge Simon Malcomber of California State University Long Beach for his phylogenetic analysis of the *rotten ear* gene. The contributions from these two gentlemen can be found in the materials and methods, results and discussion sections as well as figures 4A-F, 8B-C, and 11-C. I thank you both immensely for your help on this project.

ABSTRACT OF THE THESIS

Positional cloning and characterization of the *Rotten Ear* (*Rte*) gene in *Zea mays*

by

Ma Zara Emilia Marañon Tabi

Master of Science in Biology

University of California, San Diego, 2012

Professor Robert Schmidt, Chair

Yields in agriculturally important crops such as maize (*Zea mays*) depend on the normal growth of their flowering structures, making the understanding of inflorescence development a worthwhile undertaking. Through the analysis of ethyl methanesulfonate (EMS)-mutagenized maize populations, we identified a novel recessive mutant, *rotten ear* (*rte*), impaired in the development of inflorescences. Ears in *rte* mutants arrest during development and exhibit a brown or "rotten" appearance at

the tip. In addition, the mutant plant is sterile and fails to develop fully fertile inflorescences.

I mapped the *rte* mutant on chromosome 1, and successfully isolated the *Rte* gene through a map based cloning approach. Sequence and phylogenetic analyses showed that *Rte* is similar to the *Arabidopsis thaliana BOR1* gene, suggesting that *Rte* may encode a boron transporter responsible for boron efflux. Although a notable phenotype was only detected in the inflorescences, the *Rte* gene is expressed in both vegetative and reproductive tissue, and *in situ* hybridizations show localized *Rte* expression around the vascular tissue. Moreover, transient expression assays in tobacco (*Nicotiana benthamiana*) cells show the RTE:YFP fusion protein sequestered to what appears to be the plasma membrane. Maize also has an *Rte* paralog, *Rte-Like* (*Rte-L*), which was expressed in identical locations as *Rte*. Since the symptoms of boron deficiency are very diverse, it has been a challenge to determine the specific functions of boron in inflorescence and floral development. Because of this, we are investigating the role that the *Rte* gene plays during the development of maize inflorescences.

INTRODUCTION

Questions of development, such as those regarding the control of cell growth, differentiation and organogenesis, have intrigued scientists for many decades. Elucidating the developmental process in plants is particularly interesting from both a scientific as well as an agricultural standpoint. Fruit and grain yields in economically important crops such as maize, rice and tomato, for example, are dependent on the normal growth of their respective flowering structures. This makes the study of the complex pathways involved in their formation an especially worthwhile endeavor. Thanks to advances in genetics and molecular biology, we have been able to make great strides in our understanding of reproductive development in plants. Despite our progress, however, there are still many questions that remain unanswered. With additional understanding of these processes, it may be possible to further augment crop production and quality.

Zea mays as a model organism for genetic studies

Although the monocot maize (*Zea mays*) does not offer the benefit of a small stature, short lifecycle, and relatively small genome size possessed by most model organisms, such as *Arabidopsis thaliana* or *Drosophila melanogaster*, it still has some key characteristics that make it an excellent research subject in fields such as developmental biology, agronomy, plant pathology, and genetics. In addition to its vigor, large seed set, and diverse morphological differences within the species, maize provides researchers with a vast collection of interesting vegetative and reproductive

mutants to study (Bennetzen and Hake, 2009). Moreover, due to the recent completion of the entire genome sequence of the B73 inbred line, studies in genetics and developmental biology as well as many other fields in maize have advanced immensely (Schnable et al., 2009).

Aside from being an important agricultural staple in its own right— the most widely grown crop in the Americas, with a planted area of about 92.3 million acres in the United States alone in 2011, bringing in billions of dollars in revenue (USDA: National Agricultural Statistics Service, 2011)—as a member of the Poaceae or "true grasses" family, maize possesses a genetic colinearity with other economically important grasses such as wheat (*Triticum* spp.), rice (*Oryza sativa*), sorghum (*Sorghum bicolor*) and barley (*Hordeum vulgare*), among many others (Strable and Scanlon, 2009). This means that the studies and conclusions made in model plants such as maize can be useful for understanding common processes in other closely related species.

Basic morphology of maize inflorescences

When angiosperms, or flowering plants, transition from a vegetative to a reproductive state, they produce a structure composed of a cluster of flowers, generally known as an inflorescence. The flowers contain the reproductive organs necessary to produce one or more seeds, oftentimes embedded within the fruit. Unlike most flowering plant species that generate perfect flowers—having both male and female floral organs in the same flower—maize is considered a monoecious plant, meaning that instead it produces two distinct inflorescence structures, the tassel and

ear, which bear separate male and female flowers, respectively (Vollbrecht and Schmidt, 2009). While the development of the tassel and ear begin in a similar manner, which will be discussed in a later section, the two structures are noticeably different upon maturity. Despite this partition of male and female structures, maize is still regarded as a significant model for floral development in other grass species.

The tassel is found at the apex of the mature maize plant and can possess a variable number of long branches at its base (Figure 1A). Inserted on these branches, as well as on the central spike, are many short branches referred to as spikelet pairs. Each spikelet pair is composed of a pedicellate and a sessile spikelet, the basic component of grass inflorescences (Figure 1A, bottom insert) (Vollbrecht and Schmidt, 2009). Each tassel spikelet, encased by two sterile bracts called glumes, contains two male flowers, or florets. Floral organs include the lemma, palea, and lodicules (all non-reproductive, grass specific organs; Whipple et al., 2004) and the stamens, which develop and release the pollen (Figure 1A, top insert). Maize ears lack long branches, and are located at the ends of compressed axillary branches formed in the axils of leaves (Figure 1B). Like tassels, ears also possess spikelet pairs, but they are morphologically different from those found in the tassel. While the ear spikelets also have an inner and outer glume, lemma, palea and lodicules, one of the two florets degenerates, leaving one floret containing the pistil, which houses the ovary (Figure 1B, insert).

Roles of meristems in maize development

In maize as well as in other higher order plants, it is the meristematic tissue that gives rise to the vegetative and reproductive organs distinguishable in a mature plant. Meristems are populations of undifferentiated, actively dividing cells that are capable of reproducing themselves, oftentimes referred to as the "stem cells" of a plant due to these qualities. Upon receiving certain cellular cues from neighboring cells, meristems are capable of differentiating cells off to their flanks that proceed to form specific plant structures (Raven et al., 2005). Depending on the type of structure it produces and its location within the plant, a meristem is designated with a specific identity that may undergo changes throughout development. The shoot apical meristem (SAM) and the root apical meristem (RAM), which form during embryogenesis, remain located at the tips of shoots and roots respectively, and are responsible for primary growth on the apical/basal axes. Axillary meristems, on the other hand, are formed post-embryonically in the axils of leaves, and are responsible for secondary axes of growth, such as the formation of lateral branches and flowers.

In maize, the SAM and axillary meristems are responsible for vegetative development with the formation of stems, leaves and tillers (lateral branches), until the change from vegetative to reproductive development occurs. At this point, the uppermost SAM transitions into an inflorescence meristem (IM), that is committed to the development of the tassel inflorescence and the creation of specialized axillary meristems (Figure 2A). At the beginning of tassel formation, the IM produces several branch meristems (BMs), which are responsible for the formation of the tassel branches located at the base of a mature tassel (Figure 2B). Subsequent meristematic

tissue formed in organized rows by the IM and the BMs are committed to the formation of the spikelet pairs and are known as spikelet pair meristems (SPMs). Following the formation of a short branch, each SPM develops into two spikelet meristems (SMs) (Figure 2C). The SM produces the glumes and then proceeds to develop two floral meristems (FMs). These FMs are responsible for forming the remaining floral organs, with pistil development arresting prior to floral maturity, producing two staminate (male) florets per spikelet.

The development of the ear proceeds in a similar fashion, but with a few key differences. The IM exclusively forms multiple rows of SPMs so that mature ears are lacking long branches. Reproductive development then follows the same steps described in the tassel until the formation of the two FMs from each SM. One of the developing florets aborts, as well as all of the male stamens, resulting in one pistillate (female) floret per spikelet (Figure 2D) (Cheng et al., 1983; McSteen et al., 2000; McSteen and Leyser, 2005; Vollbrecht and Schmidt, 2009).

Genes involved in the early steps of maize inflorescence development

In our lab, we use the rich genetic resources of maize to identify new genes regulating inflorescence development and plant architecture. A great deal of work has already elucidated the role of several genes involved in this process, in particular during axillary meristem initiation in both ear and tassel development.

Floral initiation and development in plants are known to be highly dependent on a set of chemical signaling molecules, collectively known as plant phytohormones, in which auxin plays a major part (Vanneste and Friml, 2009). Auxins are a class of

aromatic compounds derived from the amino acid tryptophan. They are key to many other processes within the plant, for example, the response to light and gravity. The pivotal role of auxin in maize axillary initiation and development became evident through the study of a number of inflorescence mutants. Overall classic genetic approaches were instrumental in identifying several maize genes involved in different aspects of auxin biology. The *sparse inflorescence1* (*spi1*) mutant, for example, has a significant reduction in branch and spikelet number in the tassels, as well as smaller ears with fewer kernels. Cloning and phylogenetic analysis revealed that *Spi1* encodes a flavin monooxygenase highly similar to genes in the *YUCCA* (*YUC*) family of *Arabidopsis*, which play a key role in auxin biosynthesis (Gallavotti et al. 2008). *Vanishing tassel2* (*vt2*) is another gene associated with auxin biosynthesis, and is a co-ortholog of the *Arabidopsis TRYPTOPHAN AMINOTRANSFERASE OF ARABIDOPSIS1* (*TAA1*) gene, according to phylogenetic analysis. In addition to being significantly shorter than wild-type plants at maturity, *vt2* mutants possess a severely barren tassel, with no lateral branching or spikelets (Phillips et al., 2011).

The *barren stalk1* (*ba1*) mutant phenotype is particularly striking because, in severe alleles, both vegetative and reproductive branches are absent, suggesting a crucial role in axillary meristem formation (Ritter et al., 2002). *Ba1* encodes a basic helix loop helix transcription factor necessary for axillary meristem initiation (Gallavotti et al., 2004), that may function downstream of polar auxin transport, based on *in situ* hybridizations of young inflorescences treated with the auxin transport inhibitor N-1-naphthylphthalamic acid (NPA) (Wu and McSteen, 2007). Based on expression data and genetic analysis, normal levels of *Ba1* expression are also

dependent upon the presence of the transcriptional regulator *Barren stalk fastigiate1* (*Baf1*) (Gallavotti et al., 2011). Additionally, BA1 protein has been revealed to interact with BARREN INFLORESCENCE2 (BIF2) (Skirpan et al., 2008). *Bif2* encodes a serine-threonine kinase, which phosphorylates BA1 in vitro. Similar to the mutants previously discussed, *bif2* mutants have defects in floral development as well. BIF2 has also been shown to phosphorylate and influence the localization of ZmPIN1a, a maize homolog of the Arabidopsis auxin efflux transporter PINFORMED1 (PIN1) (Skirpan et al., 2009; Galweiler et al., 1998). Previous studies with ZmPINa:YFP fusion proteins have demonstrated that all branching events during maize development, such as those seen during the formation of axillary meristems in both ear and tassel, are marked by the establishment of auxin response maxima and by the upregulation of ZmPIN protein expression. Those studies revealed that the role of polar auxin transport in this pathway is fairly conserved between maize and *Arabidopsis* (Gallavotti et al., 2008).

Basics of plant nutrition

Plant phytohormones are not the only components needed for proper inflorescence development. The acquisition of nutrients from the surrounding environment plays a crucial role as well. Because plants are able to incorporate carbon utilizing light energy, CO_2 and H_2O, the nutritional needs of plants are fairly simple in comparison to those of animals. Over 60 chemical elements have been identified in a variety of plant species. However, not all are essential to the proper development, metabolic function, and overall survival of the plant (Raven, et al. 2005). The essential

elements are generally divided into two categories-- macronutrients and micronutrients—and are taken up through the root system.

As the name suggests, the macronutrients, which include nitrogen (N), sulfur (S), phosphorus (P), potassium (K), magnesium (Mg), and calcium (Ca), are needed in significantly larger amounts (≥1000 mg/kg of dry matter) relative to other elements. These elements serve as vital components in macromolecules such as polypeptides and nucleic acids, as well as cofactors in key enzymes and in plant pigments such as chlorophyll. Plant micronutrients include molybdenum (Mo), nickel (Ni), copper (Cu), zinc (Zn), manganese (Mn), chlorine (Cl), iron (Fe) and boron (B), and while they are needed in only trace concentrations (≤100 mg/kg of dry matter), the specific enzymatic, structural, ionic, and regulatory functions they provide are no less significant. Depending on the plant species, the specific amounts needed of these nutrients may vary, and additional elements may be regarded as essential as well (Raven, et al. 2005).

Though these elements are essential, the plant has to ensure they are present in the correct amounts to avoid symptoms of deficiency or toxicity. While most toxicity and deficiency symptoms appear during the vegetative development of the plant, and can include stunted growth, leaf curling, reduced development of chlorophyll (chlorosis) and the formation of spots of dead tissue (necrosis), deficiencies in a few key micro and macro nutrients have been shown to also affect floral and fruit development, and therefore crop yields. For example a deficiency of nitrogen, which serves as a vital component in the synthesis of proteins and nucleic acid, causes early maturity and reduced crop quality in addition to general chlorosis and stunted growth.

Plants deficient in zinc, which is needed for proper growth hormone production, experience poor flowering and low seed set, in addition to various vegetative symptoms (McCauley et al., 2003). Boron, naturally present in the soil as boric acid (H_3BO_3), has been characteristically known to affect reproductive tissue when deficient, even when vegetative symptoms are absent (Dell and Huang, 1997).

Boron and plant development

Although the metalloid boron has a relatively low natural abundance in comparison to other major elements, representing only 0.001% of the Earth's crust by mass (Argust, 1998), it is an essential plant micronutrient. Most studies of boron performed in plants focuses on its role in the formation of the cell wall. The pectin rhamnogalacturonan II (RGII), a complex polysaccharide that serve as a major structural component in higher plant cell walls, has been shown to cross link via borate-diol ester bonds (Kobayashi et al., 1996). Under conditions of boron deprivation, plants were shown to have a reduction of cell-wall elasticity (Findeklee and Goldbach, 1996) as well as altered cell wall porosity due to a decrease of RGII dimerization (Fleischer et al., 1999). However, it is the effect that boron deficiency has on reproduction that is more compelling and elusive, both in a scientific and agricultural sense. Oftentimes, crops grown on soil with low amounts of boron show no symptoms during vegetative growth, but as plants mature, reductions in yield and fruit/seed quality can be observed (Dell and Huang, 1997).

In a study monitoring the effects of boron deficiency (0.013 ppm B) during maize growth, Agarwala et al. observed delay and suppression of growth of both male

and female floral organs, and a decrease in the quantity and germination quality of pollen, which also showed altered enzymatic activity (Agarwala et al., 1981). Severe deficiencies in boron (0.0026 ppm B) resulted in lack of floral development altogether. In a similar study in wheat, Huang et al. noted analogous results. By removing boron from the growth media they noted changes in floral development and yield, and determined that floret fertility is most sensitive to the depletion of born during the initial appearance of the flag leaf up until 2±3 days after its full emergence (Huang et al., 1999). Comparable to the results of Agarwala et al. in maize, wheat grown in boron deficient conditions showed arrested anther development and decreased pollen viability, in addition to reduced female floret fertility and overall grain count. How boron limitations are causing such symptoms in reproductive development has yet to be determined.

In the model plant *Arabidopsis thaliana*, the female-sterile mutant *bor1-1*, shows increased sensitivity to boron deficiency and reduced boron content in leaves and inflorescences (Noguchi et al., 1997). The *BOR1* gene was cloned by Takano et al. and, based on the observation that growth impairment is more apparent in the shoots and floral organs versus the roots, it was speculated that the wild-type *BOR1* gene played a role in the transport of boron rather than in the structural integrity of the plant cell wall (Takano et al., 2002). This hypothesis was confirmed by transport measurement assays in *A. thaliana* and budding yeast (*Saccharomyces cerevisiae*), as well as by the presence of ten putative transmembrane domains in amino acid sequence analysis (Takano et al., 2002). More specifically, they were able to determine that the BOR1 protein was involved in efflux transport, exporting boron out

of root tissue and into the xylem tissue of the main vascular system for delivery to the shoots, making *BOR1* the first identified boron transport gene in higher organisms (Takano et al., 2002). Additional research by Takano et al. demonstrated that *BOR1* is regulated post-transcriptionally under conditions of elevated boron levels, via endocytosis of the BOR1 protein and subsequent protein degradation (Takano et al., 2005). It was later seen in follow up experiments that the overexpression of the wild-type *BOR1* gene, using the cauliflower mosaic virus 35S RNA promoter, caused improved boron translocation and seed yield under boron-limited conditions, suggesting the possibility of cultivating plants that can tolerate low boron supply (Miwa et al., 2006).

In major crops, proper boron nutrition is critical for obtaining not only high yields but high produce quality as well. The inability to take up critical amounts of the metalloid due to poor soil quality has become a major agricultural problem in many parts of the world-- the productivity of 132 crops in nearly 80 countries (Shorrocks, 1997) has been impeded due to deficiency in boron, making boron deficiency more widespread than deficiencies of any other plant micronutrient (Gupta, 1979). Such boron deficient soils can be classified as strongly weathered, coarse textured, shallow or other qualities that allow for quick leaching and run-off. Conversely, arid regions experiencing little to no rainfall can possess toxic levels of the metalloid (Shorrocks, 1997). While fertilization is one option to alleviate poor soils, the production of such chemicals is costly and can have negative effects on the environment (Miwa et al., 2006). Because the symptoms of boron deficiency are very diverse and most of which are accredited to secondary effect (Shorrocks, 1997), it has been a challenge in the

fields of plant nutrition and physiology to determine most of the specific functions of boron in vegetative development, but more importantly inflorescence, floral, and fruit development. By elucidating boron transport and the role of boron in plant growth, it may be possible to alleviate deficiency problems and increase crop production in certain areas of the world.

Thanks to recent efforts by several research groups a series of genes involved in tassel and ear development have been identified, and they have begun to shed light on the various pathways required for axillary meristem development and for the early steps of inflorescence formation. However, our knowledge is still limited. To further our understanding of the molecular mechanisms regulating axillary meristem initiation and development in maize, we started to analyze a collection of over 130 mutants defective in ear and/or tassel development, with the goal to ultimately map some of these mutations, and to clone and characterize the affected genes. Through this classical genetic approach, we hope to identify new genes involved in maize inflorescence development that could increase our knowledge of these processes. My research project continues this ongoing analysis, and resulted in the identification of a new gene required for proper inflorescence development in maize.

Figures 1 and 2 were provided by committee chair Dr. Robert Schmidt and previously published in “Development of the Inflorescences” by Vollbrecht, E., and Schmidt, R. (2009). This chapter can be found in Handbook of Maize: It's Biology,

Bennetzen, Jeff L., and Hake, Sarah C. eds., (New York, New York: Springer) pp. 13-40.

MATERIALS AND METHODS

Phenotypic Analysis

Tassel measurements were taken after two rounds of back crossing *rte-1* and *rte-2* with inbred lines Mo17 and A619, respectively. Tassel length was measured as the distance between the first tassel branch to the tassel tip, while branch length was determined by the four longest branches of tassel being measured. Branches were defined as possessing greater than two spikelets. The student's *t* test was used to determine statistical significance.

SEM Microscopy

Samples were fixed with 2% paraformaldehyde and 3% glutaraldehyde in 0.1M cacodylate buffer at 4°C for 24 hours. Samples were then rinsed in deionized water and post-fixed in 2% aqueous osmium tetroxide followed by dehydration in a graded ethanol series up to 100% ultra-pure ethanol and dried using a Denton DCP-2 critical point dryer (Denton Vacuum, LLC, Moorestown, NJ). When dried, the samples were placed onto adhesive coated aluminum stubs, sputter coated (Denton Desk II sputter coater, Denton Vacuum, LLC, Moorestown, NJ) with palladium/gold alloy, and imaged using a JEOL 5800LV SEM (Japan Electron Optics Laboratory, Peabody, MA) at 10kV with a SIS ADDA II for digital image capture (Olympus Soft Imaging Systems Inc., ResAlta, Golden, CO).

Positional Cloning of the *rotten ear* (*rte*) mutant

The *rte* mutants (Table 1) were initially identified in ethyl methanesulfonate (EMS) mutagenized M2 families generated by the Maize Inflorescence Project (http://www.maizegdb.org/mip/MIP.htm). EMS treated pollen from the inbred line A632 was used to fertilize ears of Mo17 or OH43 inbred lines. The resulting M1 progeny was then self-fertilized to generate M2 segregating populations that were distributed to the community.

30 M2 plants were planted out and scored for the *rte* mutation, and a number of phenotypically wild type plants were selfed to generate an M3 population for mapping. Once the initial M3 population was planted out, an equal amount of tissue for both mutant and wild type samples were pooled. DNA was extracted from the pooled samples to be analyzed via bulk segregant analysis using the MassARRAY® system (Sequenom) at Iowa State University. Simple sequence repeat (SSR) markers were then selected from MaizeGDB (http://www.maizegdb.org) and used on individual samples to confirm the location and establish an initial genetic interval containing the *rte* locus.

DNA from an additional 248 mutants of the subsequently planted M3 population was extracted using a Mixer Mill protocol. In each 1.2 ml tube of a 96 well plate, narrow pieces of maize tissue (1.5 cm by 2.5 cm), a single 3 mm tungsten carbide bead, and 500 µl of Candela extraction buffer (100 mM Tris-HCl pH 8.0, 50mM EDTA, 100 mM NaCl, 10 mM βmercaptoethanol) were added. The plate was then subsequently shaken twice for 1 min at 25 Hz using the Retsch MM400 Mixer Mill with Tissue Lyser Adapter Set, 2x96 (Qiagen). 70 µl of 10% SDS were added to

each tube prior to a 65°C incubation for 10 minutes. 130 µl of cold 5M potassium acetate was added and then the samples were incubated on ice for 5 minutes. Using plate adaptors with a swinging bucket rotor, tubes were centrifuged for 15 minutes at 3000 rpm. Supernatant was transferred to fresh tubes and an equal volume of isopropanol and $1/10^{th}$ volume of 3M sodium acetate were added prior to a 1 hour incubation at -20°C. Tubes were then centrifuged at 3000 rpm and resulting pellets were then washed with 70% ethanol. After centrifuging for 10 minutes, supernatant was discarded and the pellets were allowed to air dry, after which 100 µl of TE (10 mM Tris and 1 mM EDTA) was added to resuspend the DNA. DNA from individuals identified as recombinant through the use of SSR markers was re-extracted using standard DNA extraction methods for subsequent analysis.

To develop new molecular markers we utilized sequence information from maize assembled genomic islands (MAGI), which are partial genome assemblies generated from genomic survey sequences of the B73 inbred line (http://magi.plantgenomics.iastate.edu/). Primers were designed to amplify and sequence selected regions in both mutant and wild type samples. Utilizing dCAPS Finder (http://helix.wustl.edu/dcaps/dcaps.html), this sequence information was used to develop new molecular markers that were used to further delimit the position of the *rte* mutation (Table 2). Syntenic regions in sorghum (*Sorghum bicolor*) were analyzed using sequence information from Phytozome (http://phytozome.net) and a candidate gene in maize was selected based on recombination frequencies of the flanking markers. See Table 2 for SSR and dCAPS maker positions and oligonucleotide sequences, and Table 3 for primers used for sequencing the candidate gene.

Cloning of *Rte* cDNA

We generated two overlapping cDNA fragments of the *Rte* and *Rte-L* coding sequence, using the primers RE-cds-F1 with RE-cds-R3 and RE-cds-F3 with RE-cds-R2 for *Rte*, RteL-cds-F1 with RteL-cds-R1 and RteL-cds-F2 with RteL-cds-R2 for *Rte-L* (Table 6). The two fragments obtained from each gene were used to obtain a fusion product in a subsequent PCR reaction using a proofreading *Taq* DNA polymerase (Phusion, New England Biolabs). The complete *Rte* and *Rte-L* coding sequences were then A-tailed and cloned into the pGEM-T Easy vector system (Promega) according to manufacturer's instructions.

Sequence Analysis and Phylogenetic Tree Construction

Comparative sequence analysis was performed with NCBI BLAST (http://blast.ncbi.nlm.nih.gov/Blast.cgi) and ClustalW2 (http://www.ebi.ac.uk/Tools/msa/clustalw2/). Hydropathy plots were constructed using the Kyte-Doolittle scale with a window size of seventeen amino acids (Kyte and Doolittle, 1982; http://www.vivo.colostate.edu/molkit/hydropathy/).

For the phylogenetic analysis of *Rte,* ninety-five *Rte*-like genes were identified through BLAST searches from several online databases. The nucleotide sequence alignment was assembled and translated into amino acid sequences using Mesquite (Maddison and Maddison, 2010), aligned using MUSCLE (Edgar, 2004), then manually adjusted using Mesquite. Bayesian phylogenetic analyses using MrBayes 3.2 (Ronquist and Huelsenbeck, 2003) on the Grethor parallel processing cluster at the University of Missouri – St. Louis consisted of two separate searches of 10 million

generations using flat priors and the General Time Reversible (GTR) model of sequence evolution, invariant sites and gamma distributed rates partitioned according to codon position (GTR + I + SS) and with trees being sampled every 1000 generations. Convergence between the two runs was determined by examining the average standard deviation of the split frequencies (0.006077). After convergence had been assured the first 25% of trees were removed as burn-in and clade credibility values estimated using MrBayes.

Reverse-Transcriptase (RT) PCR

Total RNA was extracted from 100 mg samples of maize tissue, using the Plant RNeasy Minikit (Qiagen) and treated for 30 minutes with DNAse. 20 ng of extracted RNA was used to amplify a fragment encompassing the eleventh exon of *Rte* and *Rte-L* to the 3' untranslated region (Figure 9A) with Superscript One-step RT-PCR with Platinum® Taq (Invitrogen), using primers RE-T25-F7 and RE-T25-R6 for *Rte,* and RteL-RTPCR-F1 with RteL-RTPCR-R1 for *Rte-L* (Table 6). A ubiquitin control was also run on the RNA samples to ensure uniform loading (UBQ-F and UBQ-R; Table 6). Results were visualized on a 1% agarose gel.

***In situ* Hybridization**

Using cDNA as a template, a PCR fragment was created using primers RTE-pAD-EcoRI-F1 and RTE-pAD-SalI-R2 for *Rte* and RteL-pAD-EcoRI-F1 and RteL-pAD-SalI-R2 for *Rte-L* (Table 7), which was subsequently cloned into pAD-GAL4-2.1, digested with *Eco*RI and *Sal*I, with Cold Fusion technology (System Biosciences)

following manufacturer's instructions. 20 µg of the construct were linearized with *Eco*RV for creating the antisense DIG-labeled RNA probes (Roche) with T7 RNA polymerase (Promega). *In situ* hybridization was performed as previously described (Gallavotti et al, 2011).

Transient Expression Assay

To synthesize the *Rte:YFP* and *Rte-L:YFP* transgenes, both the *Rte, Rte-L* and *YFP* coding sequences were amplified separately with the primers RTE-35s/pBJ36-XhoI-F1 with RTE/YFP-R2 for *Rte*, RteL-35s/pBJ36-XhoI-F1 with RteL/YFP-R1 for *Rte-L* and YFP/RTE-F2 with YFP-35s/pBJ36-XhoI-R1 for *YFP* (Table 8) using proofreading *Taq* DNA polymerase (Phusion, New England Biolabs). *Rte* and *Rte-L* fragments were each combined with *YFP* in a second round of PCR and the resulting amplicons were cloned into pBj36+2x35S cut with *Xho*I using Cold Fusion technology (System Biosciences). The *35S::Rte:YFP* cassette was isolated using *Not*I digestion and cloned into the T-DNA binary vector pML BART (Gleave, 1992). Similarly, a *35s::YFP* construct was created to serve as a control. The corresponding *Agrobacterium* tobacco leaf infection was performed as described previously (Gallavotti et al, 2011).

Complementation Test

To create the transformation constructs, the native *BOR1* promoter region (1158 bp upstream of the *BOR1* start codon; Takano et al., 2002) and the *Rte* coding sequence were amplified separately with the primers BOR1-RTE-3xHA/pBJ36-XhoI-

F1 with BOR1/RTE-R1 and RTE/BOR1-F1 with RTE-3xHA/pBJ36-XbaI-R1 (Table 9) using proofreading *Taq* DNA polymerase (Phusion, New England Biolabs). For the *pBOR1::Rte* construct, both fragments were combined in a second round of PCR and the resulting amplicon was cloned into pBj3635S+2XYPetM+3xHA via *Xho*I and *Xba*I cut sites using Cold Fusion technology (System Biosciences). Through digestion of pBj3635S+2XYPetM+3xHA with *Xho*I and *Xba*I, the 2XYPetM+3xHA fragment was removed. For the *35S::Rte* construct, the *Rte* coding sequence was amplified with proofreading *Taq* DNA polymerase (Phusion, New England Biolabs) using the primers RTE-35s/pBJ36-XhoI-F1 and RTE-35s/pBJ36-XhoI-R1 (Table 9). The amplicon was subsequently cloned into pBJ36+2x35s via *Xho*I cut site with Cold Fusion technology. After sequencing, the *pBOR1::Rte* and *35S::Rte* cassettes were isolated using *Not*I digestion and each cloned into the T-DNA binary vector pML BART (Gleave, 1992). *bor1* T-DNA insertion mutants were obtained from lines at the Salk Institute (Alonso et al., 2003). *Arabidopsis* was transformed using the floral dip transformation method described in Clough and Bent, 1998.

Mature *Rte* mRNA was detected via RT-PCR using primers Rte-cds-F3 and Rte-cds-R2. ß-*Tubulin* was also amplified as a control using primers TUB+ and TUB- (Table 10). To genotype *bor1* transformants, three primers were used: A band detected with 037312-F and LBb 1.3, but not using 037312-F and 037312-R indicated a *bor1* T-DNA insertion mutant (Table 11).

I would like to acknowledge the work of Michael Muszynski of Iowa state University, who not only provided us with SEM imagery of the young ear

primordium, but additional *rotten ear* alleles as well. I would also like to acknowledge Simon Malcomber of California State University Long Beach for his phylogenetic analysis of the *rotten ear* gene. The contributions from these two gentlemen can be found in the materials and methods, results and discussion sections as well as figures 4A-F, 8B-C, and 11-C. I thank you both immensely for your help on this project.

RESULTS

I. The *rotten ear (rte)* mutant is impaired in tassel and ear development

One of the main goals in our lab is to identify new genes involved in axillary meristem formation. Thus, undertaking a classical genetic approach, we analyzed maize ethyl methanesulfonate (EMS)-mutagenized populations to screen for mutants affected in inflorescence development, with the goal to ultimately map these mutations. These mutants were generated in different genetic backgrounds by the Maize Inflorescence Project (http://www.maizegdb.org/mip/MIP.htm), and the seeds were provided by the Maize Genetics Stock Center. These populations were first analyzed, and the putative mutant phenotypes were classified according to specific classes. We preliminary mapped several of these mutants by bulk segregant analysis, using the MassARRAY® system (Iowa State University). This system is a high-throughput technique that utilizes a MALDI-TOF mass spectrometer to quantitatively distinguish differences between wild-type and mutant DNA at more than a thousand single nucleotide polymorphism (SNP) based markers distributed throughout the maize genome (Liu et al., 2009). Markers demonstrating a bias towards the mutant background are regarded as "linked" to the mutation.

Among those analyzed, a group of recessive mutants, designated as *rotten ear (rte)* based on their similar phenotype, were rough-mapped to the same region on the upper arm of chromosome 1 in bin 1.05 (bins are defined as arbitrary genetic units of maize chromosomes and correspond to approximately 20 centimorgans). While a number of other maize mutants were also analyzed, screened, and mapped in a similar

manner during the course of my thesis work (Table 1), I focused my efforts on mapping the *rte* mutants due to their novel phenotype and the possible availability of multiple independent alleles for cloning. The *rte* mutants listed in Table 1, 04HI-Mo17XA632GN-16, 04HI-Mo17xA632GN-128 and 04HI-OH43xA632GN-190, eventually turned out to be allelic based on fine-mapping studies, with two of the mutants possessing the same allele. As a result, we designated 04HI-Mo17XA632GN-16 and 04HI-Mo17xA632GN-128 as *rotten ear-1* (*rte-1*) and 04HI-OH43xA632GN-190 as *rotten ear-2* (*rte-2*) respectively.

In wild-type ears, multiple, uniform rows of axillary meristems are present. These axillary meristems progress in identity from spikelet pair meristems, to spikelet meristems, to floral meristems until finally mature florets are formed and the silk grows, ready for pollination (Figure 3A). In *rte* mutants, this normal morphology is not seen, and instead ears are smaller and posses fewer developed florets that in most cases have a brown or "rotten" appearance at the tip (Figure 3B-D); hence the name "*rotten ear*." Generally, *rte-1* mutants display a more severe phenotype where in extreme cases all florets fail to form, leaving the ear dramatically reduced (Figure 3C, D). *rte-2* mutants were found to be milder in comparison, with the "rotten" phenotype affecting a smaller portion of the ear tip (Figure 3B). Within the same allele, variations in severity can be seen, indicating an environmental effect may be involved in determining the phenotype observed.

To establish whether this phenotype is the result of a failure to initiate meristematic tissue or to maintain meristematic growth, scanning electron microscopy (SEM) images of young ear primordia were taken at different points in development,

and analyzed. *rte* mutant ears appear to be nearly indistinguishable from that of wild-type at early stages, and the formation of normal spikelet pair meristems and spikelet meristems from the inflorescence meristem can clearly be observed (Figure 4A-D). In addition, *in situ* hybridizations on *rte* ears of the *Knotted1* (*Kn1*) gene, a homeobox transcription factor involved in meristem maintenance (Kerstetter et al., 1997), show the characteristic *Kn1* expression in meristematic tissue, suggesting the *rte* mutant can successfully initiate meristematic tissue developed at early stages (Figure 4G). However as the ear progresses towards more advanced stages, the "rotten" phenotype manifests itself (Figure 4E, F). Meristems are still seen in mutant ears, but the meristematic tissue established later in development as well as the inflorescence meristem itself appear malformed and withered, and the cessation of further meristem formation is presumed. This is supported by the lack of strong *Kn1* expression at the tip where the inflorescence meristem should be located. Expression is still seen in the spikelet pair meristems that immediately flank the region, suggesting the inflorescence meristem had deteriorated (Figure 4G, H arrows). This lack of phenotype at earlier stages indicates that *rte* function is required during late inflorescence development and suggests that the mutant phenotype is a result of the failure to maintain growth of meristematic tissue.

Despite the "rotten ear" moniker, a notable phenotype is also seen in the *rte* mutant tassel. In normal tassels, which develop in a progression similar to that of the ears, several primary branches can grow from the base of the central spike. Each branch is covered in a number of spikelets, which house the male florets responsible for pollen production (Figure 5A). *rte* tassels possess fewer and shorter branches as

well as fewer spikelets in comparison to wild-type plants (Figure 5B-D). In extreme cases the central spike, the branches, and the spikelets completely fail to form. Similar to observations in the ears and confirmed by quantitative tassel measurements (Figure 6A, B and Table 12), the *rte-1* allele (Figure 5C, D) appears to have a more severe phenotype, with significantly shorter tassels and branches in comparison to the wild-type, more so than the *rte-2* allele (Figure 5B), which possesses a milder tassel phenotype. The spikelets that do form appear to retain all of the basic structural components of the spikelet—the inner and outer glume, lemma, palea, lodicule and stamens (Figure 7B). However upon closer inspection of the mutant stamens, little to no pollen is observed. While the viability of *rte* pollen has yet to be confirmed, selfing of mutants and outcrosses were always unsuccessful in field conditions, suggesting that both ear and tassel fertility are compromised and that *rte* is a sterile mutant.

II. *rte* encodes a putative boron transporter

By identifying the mutated gene through a map-based cloning strategy, we can learn about the protein it encodes and its putative function, as well as investigate its role in inflorescence development. The *rte* mutant was originally identified segregating in small M2 populations obtained from the Maize Genetics Stock Center. Given the sterile nature of the mutation we propagated the mutant by selfing wild-type looking plants. M3 populations segregating the *rte* mutant phenotype were subsequently used for mapping purposes. As mentioned previously, the *rte* mutation was rough mapped to bin 1.05 on the upper arm of chromosome 1 utilizing bulk segregant analysis of a pooled sample of 31 04HI-Mo17XA632GN-16 mutants as well

as a pooled sample of 40 04HI-Mo17XA632GN-157b mutants (Figure 8A top). The two mutant pools were compared with a corresponding wild-type pool composed of an equal number of plants. This preliminary map position was then confirmed through the use of simple sequence repeat (SSR) markers selected from MaizeGDB (http;//www.maizegdb.org) to define a genetic interval encompassing the *rte* locus (Table 2).

To expand the mapping population and minimize the region containing the *rte* locus, additional M3 seeds segregating for the 04HI-Mo17XA632GN-16 mutant were subsequently planted out, scored and analyzed, resulting in a total of 319 mutant plants. During our mapping, we soon realized that the mutant phenotype was associated with polymorphisms found in Mo17, rather than the mutagenized A632. The use of additional SSR markers, and of newly developed molecular markers based on available genome sequence information at MAGI (Maize Assembled Genomic Islands) allowed us to restrict the region containing the rte locus to a 3.2 Mb region on contig 31 between markers MAGIv4_1364 and MAGIv4_55889 (Figure 8A).

In order to check for conserved synteny, which is the presence of common genes in specific chromosomal region among different species (thus indicating an evolutionarily common chromosomal segment), the loci corresponding to the flanking markers MAGIv4_1364 and MAGIv4_55889 were located in sorghum (*Sorghum bicolor*) using the Phytozome online database (http://www.phytozome.net). Sorghum is a close relative to maize, and has a considerably smaller genome (700 Mb versus 2,500 Mb; http://www.phytozome.net), and at the time of analysis it had a better gene annotation in comparison to the available maize genomic sequences. The

corresponding loci encompassed a 0.68 Mb interval on chromosome 8 of sorghum, which was found to be syntenic to the established window on chromosome 1 in maize. We therefore analyzed the sorghum sequence in this interval for the presence of predicted coding genes. Thirty-four predicted genes were found in sorghum (Figure 8A bottom) and used to identify the corresponding maize genes by searching MAGI and NCBI BLAST (http://blast.ncbi.nlm.nih.gov/Blast.cgi) databases. One of these candidate genes, *GRMZM2G166159*, encoded a putative transporter and was analyzed based on recombination frequencies of the flanking markers as well as on reports describing maize under boron-limited conditions (Figure 8B) (Agarwala et al., 1981). When sequenced in both the 04HI-Mo17XA632GN-16 and 04HI-Mo17xA632GN-128 mutants (*rte-1*), the locus contained a cytosine deletion at position +330 of the coding sequence, causing a frameshift and eventual truncation of the predicted amino acid sequence. The occurrence of the same lesion in two different EMS mutants strongly suggests that the mutation may have occurred in the wild-type Mo17 background. When 04HI-OH43xA632GN-190 (*rte-2*) was sequenced at the same locus, a single nucleotide change was detected at position +1,078, which produced a premature stop codon (CAA to TAA), also resulting in a truncated protein. Furthermore, two additional *rte*-like mutants provided by collaborator Dr. Michael Muszynski (Iowa State University) and designated as *rte-3* and *rte-4*, were sequenced at this locus: a base pair change encoding a premature stop codon (TGG to TGA) in the +739 position and a base pair change encoding a Ser to Leu substitution (TCA to TTA) in the +1,081 position were found, respectively. This polar to non-polar amino acid change in *rte-4* occurs in a highly conserved region among a number of similar proteins in other plant

species (Figure 8C). The occurrence of four different, independent lesions in the coding sequence of *GRMZM2G166159* in four *rte* mutants demonstrates that this locus corresponds to *Rte.*

The *Rte* gene consists of 12 exons and 11 introns, with a coding sequence of 2,130 nucleotides predicted to encode a polypeptide of 709 amino acids. Comparative sequence analysis shows strong similarity of RTE to the *Arabidopsis* BOR1, with a 91% amino acid similarity. As mentioned in the introduction chapter, BOR1 had already been well characterized as a transporter protein, specifically involved in the efflux of boron into xylem tissue, but also having some resemblance with bicarbonate transporters of animal origin (Takano et al., 2002).

III. *Rte* is expressed in vascular tissue

Understanding where a gene is expressed is a key piece of information in determining the role it plays in the plant. To first establish in which tissues the *Rte* gene was expressed, qualitative reverse-transcriptase (RT) PCR was performed (Figure 9A). *Rte* mRNA was detected in ear and tassel tissue as well as root, leaf, endosperm and embryo (Figure 9B). These results indicate that *Rte* is generally expressed in both vegetative and reproductive tissues.

To further investigate the specific domain of *Rte* expression, mRNA *in situ* hybridizations were performed using an antisense probe. In transverse sections of young maize seedlings, strong expression was observed mainly in the vasculature, the tissue responsible for the transport of water, nutrients and photosynthates throughout the plant. More specifically, expression was seen in the cells surrounding the xylem

tissue, the section of the vascular bundle central to the shoot axis, involved in the root to shoot transport of water and minerals (Figure 10A-C). Similar expression patterns were detected in young ear longitudinal sections, where high mRNA levels were also observed in the vasculature, though xylem and phloem were unable to be distinguished (Figure 10D, E).

IV. Subcellular localization of the RTE protein

To examine the subcellular localization of the RTE protein, we made a *RTE:YFP* reporter construct under the control of the Tobacco Mosaic Virus 35S promoter. This construct was introduced into *Agrobacterium tumefaciens* that was subsequently injected into tobacco (*Nicotiana benthamiana*) leaves for a transient expression assay. The RTE:YFP fusion protein to localize mainly to the plasma membrane of the plant cell when visualized via florescence microscopy (Figure 11A). Some slight signal was detected within the cell as well, which may correspond to the tonoplast of the vacuole (Figure 11A arrow). This was in contrast to the signal observed with the *35S::YFP* construct, which was more homogenously distributed throughout the cell, including the nucleus and the cytosol, indicated by fluorescence in cytoplasmic strands (Figure 11B). Similar results were reported with transient assays of GFP:BOR1 fusion protein (Takano et al., 2002). These results as well as the presence of ten putative transmembrane domains in the RTE Kyte-Doolittle Hydrophobicity plot (Figure 13B) give support to *Rte* encoding a transmembrane protein localized at the plasma membrane.

V. *Rte* is orthologous to the *BOR1* gene in *Arabidopsis*

Computer-based analysis is often utilized to investigate the phylogeny and evolution of a newly cloned gene, in order to compare it with similar genes based on BLAST searches in online databases, and to uncover any notable evolutionary relationships between genes in the same and different species. With this information, it is also possible to gain some insight about the function of the gene of interest based on genes with a strong resemblance to it. Collaborator Dr. Simon Malcomber at California State University Long Beach took a collection of 95 RTE-like proteins from a sample of land plants and performed a comparative sequence analysis, depicting a subset of 44 genes in a Bayesian tree (Figure 11C). RTE shares a strongly supported clade (1.00 posterior probability) with the locus corresponding to *Arabidopsis* BOR1 (*At2g47160*). Within this clade are two eudicot subclades, while only one monocot-exclusive subclade is seen, suggesting a duplication event had occurred within the eudicots. RTE falls within the strongly supported monocot subclade with another maize locus (*GRMZM2G082203*) as well as loci from other monocot species *Brachypodium distachyon,* sorghum*,* and rice. Additionally, the rice locus (*Os12g37840*) had been previously characterized as a transporter and BOR1 ortholog, OsBOR1 (Nakagawa et al., 2007). BLAST searches show that the second maize locus, *GRMZM2G082203*, had a 94% nucleotide alignment with the *Rte* gene, which translated to a 95% amino acid similarity. This suggests that in the maize genome an independent duplication event occurred at this locus, and that these two proteins may serve an identical or similar function.

VI. Preliminary analysis of the *Rte-Like* gene

The presence of an *Rte*-like (*Rte-L*) gene within the maize genome had been discussed in an earlier section, speculating that the gene had arisen from a duplication event and that it may have an identical or similar function to *Rte.* To investigate its expression pattern, qualitative RT-PCR was performed in a similar manner to *Rte*, amplifying a region encompassing the last two exons of the coding sequence as well as the 3' untranslated region. Like *Rte*, *Rte-L* mRNA was seen in ear and tassel tissue as well as root, leaf, embryo and endosperm, indicating that *Rte-L* is generally expressed (Figure 12A). *In situ* hybridization of *Rte-L* using an antisense probe for the coding sequence detected expression surrounding the vasculature of both young ear and shoot tissue (Figure 12C, E), closely resembling the expression pattern seen tissue probed with *Rte* (Figure 12B, D).

Based on Kyte-Doolittle Hydrophobicity plots of the amino acid sequence, it was hypothesized that *Rte-L* would also localize to the plasma membrane. The plot of RTE-L (Figure 13A) is very similar to that of RTE and BOR1 (Figure 13B, C), with ten putative transmembrane domains represented by ten positive-value peaks. This was confirmed though a transient expression assay, where the RTE-L:YFP fusion protein also appeared to localize to the plasma membrane of the plant cell (Figure 13D).

VII. Complementation of the *Arabidopsis bor1* mutant

If *Rte* and *BOR1* share a similar function during development, they may demonstrate functional complementation, where a wild-type copy of *Rte* would either

completely or partially rescue the defects of the *bor1* mutant. We performed a complementation test using *Agrobacterium*-mediated transformation of an Arabidopsis *bor1* mutant with the maize *Rte* gene using two different constructs. In one construct the *Rte* coding sequence was expressed under the control of the region 1,158 base pairs upstream of the *BOR1* start codon (*pBOR1*), used in previous complementation experiments performed by Takano et al., 2002. In the other, the *Rte* coding sequence was placed under the control of the strong Tobacco Mosaic Virus 35S promoter.

Initial experiments with the *pBOR1::Rte* construct resulted in 16 transformants, but none appeared to have restored the wild-type phenotype. Instead, transformants demonstrated the delayed and reduced growth as well as the decreased seed set characteristic of the *bor1* mutant (Noguchi et al., 1997) (data not shown). To check if *Rte* was expressed in these plants, we performed RT-PCR on a subset of 6 transformants, but no mRNA was observed in all individuals tested (Figure 14A). Since no other genomic regions of the *BOR1* gene were used in our construct, this suggests that the 5' region alone was not sufficient to drive expression of *Rte* in our transformants, and other elements are likely required, as previous complementation experiments with *BOR1* utilized the entire genomic sequence as well as the 3' untranslated region (Takano et al., 2002).

Experiments with the *35S::Rte* construct resulted in 19 transformants, with a subset of 8 transformants showing normal flowering and fruit formation in comparison to mutant controls planted at the same time (Figure 14B, C arrows). These preliminary results suggest that the wild-type phenotype has been restored in

the *bor1* mutants, however additional time is needed for the plants to reach maturity to verify these initial observations.

I would like to acknowledge the work of Michael Muszynski of Iowa state University, who not only provided us with SEM imagery of the young ear primordium, but additional *rotten ear* alleles as well. I would also like to acknowledge Simon Malcomber of California State University Long Beach for his phylogenetic analysis of the *rotten ear* gene. The contributions from these two gentlemen can be found in the materials and methods, results and discussion sections as well as figures 4A-F, 8B-C, and 11-C. I thank you both immensely for your help on this project.

DISCUSSION

rotten ear, a novel inflorescence mutant in maize

The identification and analysis of mutants impaired in inflorescence development can provide new insights into the pathways involved in meristem development and maintenance. Screening of EMS-mutagenized populations for such mutations led to the discovery of a new inflorescence mutant, designated as *rotten ear* due to the characteristic withered brown tip displayed by the ears (Figure 3B-D). These mutants also possessed a distinct tassel phenotype, which correlated with the severity of the ear defect (Figure 5B-D). *rte-2* (Figure 3B and 5B) possessed a milder phenotype in comparison to *rte-1* (Figure 3C,D and 5C,D), though both alleles displayed some significant variability in phenotype when grown under field conditions. Because soil and water levels are not entirely homogeneous in such settings, environmental effects may play a role in ear and tassel development of the *rte* mutant. There is also a possibility that genetic modifiers could be affecting the observed phenotype as well.

Through the analysis of SEM images of young ear primordium, we observed that the *rte* mutation is virtually indistinguishable from the wild-type ear at very early stages where the normal formation of SPMs from the IM is observed, then manifests itself at the inflorescence tip at a later stage in development (Figure 4A-D). The presence of meristematic tissue was confirmed through the expression of the meristem marker, *Kn1* (Figure 4G). This differs somewhat from inflorescence mutants that have been previously characterized in our lab, as the *rte* mutation appears to be affecting the

maintenance rather than the initiation of meristematic tissue. In SEM micrographs of *spi1* tassel primordia, for example, a drastically reduced number of BMs and SPMs were seen on the flanks of the inflorescence, resulting in a smooth appearance (Gallavotti et al., 2008). Similarly, SEM of *ba1* tassels revealed the presence of subtle bumps during early stages of development and onward, leading to the branchless phenotype (Ritter et al., 2002). These bumps were determined to be suppressed bracts and not arrested meristematic tissue, based on the lack of *Kn1* expression (Ritter et al., 2002). Despite the defects in meristem initiation in previously studied mutants, the spikelets that manage to form in *ba1* and *spi1* plants were able to shed fertile pollen (Ritter et al., 2002; Gallavotti et al., 2008). *rte* mutants are regarded as sterile due to the inability to self or outcross and set seed, once more implying a defect in proper maintenance of the florets as opposed to floret formation. Though this observation has not yet been confirmed, a pollen viability test utilizing germination medium could be administered to verify male sterility. These features of the *rte* mutant and their deviations from the phenotypes observed in other mutants we have characterized, which are involved in with the biology of the phytohormone auxin, suggested that the *Rte* gene may be part of a different additional pathway of inflorescence development.

The *Rte* gene encodes a putative boron transporter

We fine-mapped the *rte* mutant to the long arm of chromosome 1 and subsequently cloned *Rte*. *Rte* encodes a putative transporter and has a strong similarity to the previously characterized *Arabidopsis BOR1* (Figure 8B), suggesting that the RTE protein may serve the same function in maize. This hypothesis is supported by

phylogenetic analysis where *Rte* and *AtBOR1* fall under a strongly supported clade (1.00 posterior probability), along with other orthologous genes in both monocots and dicots, some of which previously characterized as boron transporters (Figure 11C) (Nakagawa et al., 2007).

We can surmise that the more severe phenotypes seen in the *rte-1* mutants could be due to a greater degree of truncation, where a premature stop codon is introduced due to a cytosine deletion at +330, while in *rte-2* the stop codon introduced at +1078 would leave more of the protein intact. This hypothesis would only be true if a protein product is produced from the *rte-1* allele, as there is a possibility that the severely truncated peptide immediately goes through a protein degradation pathway after translation, unsuitable for its task in the cell (Lodish et al., 2008). In the future, a western blot could be performed on both *rte-1* and *rte-2* mutants, utilizing primary antibodies that would target N-terminal residues of the RTE protein, as these are presumed to be intact in both alleles. Such an experiment would help determine the nature of the two mutant alleles, whether or not the phenotypes observed are due to the presence of defective proteins or simply the absence of protein.

Considering the variable phenotypes observed within the same *rte* allele as well as observations made in maize grown under boron-limited conditions, it is likely that the RTE protein is a boron transporter. The findings of Agarwala et al., who reported defects in the growth of floral organs in maize under different levels of boron deficiency initially led us to examine the putative boron transporter *GRMZM2G166159* within our mapping interval, as the *rte* mutant phenotype seemed to resemble these deficiency symptoms, such as the shriveled, aborted florets, reduced

number of pollen grain with poor germination quality, as well as shorter tassels with fewer branches (Agarwala et al., 1981). The more severe mutants could result from a defective or absent transporter compounded with the lack of available nutrients in the field soil.

While the preliminary results of our mutant *bor1* complementation assay look promising and provide some evidence for RTE's role as a boron transporter, several additional experiments could be performed to further confirm this hypothesis. Elemental profile analysis of mutant and wild-type plants via inductively coupled plasma mass spectroscopy (ICP-MS) could give us an initial idea of what substrate is being transported. If RTE is a boron transporter with a role similar to that of AtBOR1, we would expect to see a lower amount of boron in the shoots of *rte* plants compared to the wild type as observed in *Arabidopsis*, as the BOR1 protein is responsible for loading boron into the xylem at the roots, where it would be transported up the shoot and subsequently loaded out of the xylem to be distributed to the rest of the plant (Takano et al., 2002). Another possible assay that could be performed would be to complement yeast (*Saccharomyces cerevisiae*) carrying a mutation in YNL275w, a membrane protein significantly similar to BOR1 whose amino acid sequence is 50% similar to RTE. Through comparison of intracellular soluble boron levels in wild type, *ynl275w*, and *ynl275w* yeast transformed with *Rte* cDNA, we would expect a decrease of boron in wild type and *ynl275w* containing the *Rte* cDNA if RTE is involved in the efflux of boron out of the cell, as previously demonstrated in studies of *BOR1* (Takano et al, 2002).

Expression pattern and protein localization of *Rte*

Through qualitative reverse transcriptase PCR, we found that the *Rte* gene is expressed in both vegetative and reproductive tissue (Figure 9B). These results are supported by the *in situ* data, where expression is observed in both shoot and inflorescence sections (Figure 10 A-E). We detected higher levels of mRNA in the cells surrounding the vasculature, but more specifically the xylem tissue (Figure 10A-C). These expression patterns are similar to those observed in earlier experiments performed in rice *OsBOR1* and barley *Bot1*, both monocot orthologs of *AtBOR1*. Though different plant tissues were analyzed in these previous experiments, expression in these orthologs was also limited to an area surrounding the vasculature (Nakagawa et al., 2007; Sutton et al., 2007). Because a notable phenotype in maize was only observed in the inflorescences, with the data obtained in these expression analyses, we could infer that the reproductive stage of development is more sensitive to deficiencies in the substrate the RTE protein transports.

To investigate the subcellular localization of the RTE protein, a transient expression assay via tobacco injection was also performed. As expected from a putative transporter, the RTE:YFP fusion protein was localized to the membrane of the plant cell, with a majority of the signal around the cell periphery (Figure 11A). The florescence detected within the cell, suspected to indicate the tonoplast of the vacuole, may be a consequence of the overexpression of the *Rte:YFP* transgene, resulting in an excess amount of protein. Similar results were reported with transient assays of GFP:BOR1 as well as sGFP:OsBOR1 fusion proteins, which also localized to the cell membrane under conditions of boron sufficiency (Takano et al., 2002; Nakagawa et

al., 2007). Under high boron conditions (100 μM boric acid), the GFP:BOR1 fusion proteins were observed to internalize to vesicles within *Arabidopsis* root cells, as a form of post-translational modification (Takano et al., 2005).

Although we detected localization of RTE to the cell membrane *in planta*, it would be ideal to confirm these results in maize, and observe any notable cell type specific localization. This information could be obtained by creating maize transgenic plants expressing *Rte* fused to *YFP* under the control of the native *Rte* promoter.

***Rte-L*, the *Rte* paralog**

During our characterization, we noted the presence of a gene nearly identical to *Rte* in the maize genome, which we designated as *Rte-Like* (*Rte-L*). Based on phylogenetic analysis as well as nucleotide alignment (94%), it is postulated that *Rte* and *Rte-L* had arisen from the maize-tripsacum duplication event (Gaut and Doebley, 1997) that occurred independent from other monocots (Figure 11C). As a result, the two genes probably serve an identical or highly similar purpose within the plant. Preliminary RT-PCR and *in situ* results detected *Rte-L* mRNA in all regions where *Rte* would also be found, providing some evidence for functional redundancy (Figure 12A-E). Similar to RTE, the RTE-L:YFP fusion protein was also observed to localize to the cell membrane (Figure 13D).

The presence of two nearly identical genes within the maize genome expressed in identical locations raises the question of how a detectable phenotype could be observed when only one gene is mutated. One possible explanation would be a

"dosage effect," where elimination of only one of the two genes would lead to a relatively mild phenotype, affecting mainly the inflorescences as observed in the *rte* mutants, as this stage appears to be more sensitive to nutrient deficiency in maize as well as other species (Agarwala et al., 1981; Dell, 1997). In rice, which only possesses one At*BOR1* ortholog, disruption of this single gene via transposon insertion lead to a diminished size of the *osbor1* plant at maturity in addition to drastically reduced seed development in boron-limited conditions (Nakagawa et al., 2007). It would be interesting to produce an *rte/rte-l* double mutant to determine if changes in phenotype would be observed as hypothesized. An *rte-l* mutant would first have to be identified and obtained by searching insertion seed stocks such as UniformMu (http://www.maizegdb.org/documentation/uniformmu/), to see if a transposon is inserted within the *Rte-L* gene. If there were a dosage effect, a mutation in both *Rte* and *Rte-L* would most likely lead to a more severe "rotten ear" phenotype, which would probably affect vegetative growth as well.

Because of the *Rte* paralog, it is crucial to repeat *in situ* hybridizations of *Rte* and *Rte-L* with probes more specific to each of the two genes, utilizing sections of the coding sequence with high dissimilarity or the 3' untranslated region rather than the hydrolyzed coding sequences utilized in this study. The high similarity between the two genes implies that the expression patterns seen in our *in situ* data may not be solely due to just one of the paralogs. If the expression pattern does differ between the two genes, this may provide another explanation as to why a phenotype is seen when only one paralog is mutated.

The role of *Rte* in inflorescence development

While the project was initiated in hopes of filling in the gaps of knowledge regarding inflorescence development, these findings instead raise a number of new questions to answer. Most importantly, what role does *Rte*, a putative transporter, have in the development of meristematic tissue and maize floral structures? It is also reasonable to question what role boron plays in overall inflorescence development as well, and in particular in the production of reproductive structures, such as pollen grains and carpels.

While very little is known in regards to the transport of boron in maize, a great deal of work has already been accomplished in *Arabidopsis*. In addition to *BOR1,* six other homologous transporters (*BOR2-7*) have been identified, and characterization on a number of these genes has already been carried out. High boron supply was shown to cause increased levels of *BOR4*, unlike *BOR1*, and transgenic lines overexpressing *BOR4* resulted in improved growth under toxic levels of boron. These experiments indicate a role in toxicity prevention, as well as suggest possible applications for the improvement of crop yields in regions of excess boron (Miwa et al., 2006).

In addition to the BOR1 family, some members of the major intrinsic proteins (MIPs) have also been shown to be involved in the transport of boron. Unlike BOR1, the MIPs are channel proteins with little to moderate selectivity, capable of transporting other small molecules, most commonly water (Bienert et al., 2008). Expression of *NOD26-like intrinsic protein5;1* (*NIP5;1*) was observed to increase under boron deficiency and similar to *bor1-1*, the *nip5;1* mutants also demonstrated defects in reproductive development (Takano et al. 2006). Transportation assays in

Xenopus laevis eggs confirmed the transport of water and boron, but due to its channel properties, may be capable of transporting additional molecules as well. A model of boron transport from the soil into the xylem was proposed by Takano et al., based on the data obtained from their *BOR1* and *NIP5;1* studies. Boron passively enters the symplasm of the root system through NIP5;1 and, once past the casparian band, is subsequently loaded into the xylem via active transport by BOR1 (Takano et al., 2008). A similar pathway was proposed in rice with *OsNIP3;1* and *OsBOR1* (Takano et al., 2008), suggesting boron uptake from the soil is relatively conserved among monocots and dicots.

NIP6;1, another MIP involved in the transport of boron, is particularly interesting, as transgenic lines expresssing*1-ß-glucuronidase* (*GUS*) under the control of the *NIP6;1* promoter showed strong staining of nodes, young leaf petioles, and the base of flowers, indicating specific expression as well as a greater need for boron in these areas of growth. Interestingly, under conditions of boron deficiency, T-DNA insertion mutants of *NIP6;1* show a loss of apical dominance, a phenomenon regulated by auxin, where the growth of the axillary buds is inhibited (Tanaka et al., 2008). These results suggest a correlation between areas of high boron and high auxin, thus providing a possible connection between the micronutrient and inflorescence development.

As mentioned in a previous chapter, because the responses to boron deficiency are varied and numerous, it has been a difficult task to determine where exactly boron functions within the plant system. While the role of boron in cell wall synthesis has been extensively researched (Kobayashi et al., 1996), many hypotheses have been

proposed for other postulated roles for boron, including but not limited to: cell wall structure, DNA synthesis, RNA metabolism and indole acetic acid (IAA) (auxin) metabolism (Loomis and Durst, 1992).

Despite these unanswered questions, the *Rte* gene might have some potential for biotechnological application. Similar to experiments performed in *Arabidopsis* (Miwa et al., 2006), overexpression of *Rte* in maize by placing the gene under a constitutive promoter could lead to transgenic plants that could tolerate areas of boron deficiency. This is significant due to the importance of boron during reproductive growth and fruit development in maize and other plant species (Agarwala et al., 1981; Dell and Huang, 1997). Ideally, this could result in improved seed yields and an environmentally conscious alternative to chemical fertilization in regions such as India and eastern and southern China (Shorrocks, 1997) where poor soil quality is a major problem and a hindrance to crop production.

I would like to acknowledge the work of Michael Muszynski of Iowa state University, who not only provided us with SEM imagery of the young ear primordium, but additional *rotten ear* alleles as well. I would also like to acknowledge Simon Malcomber of California State University Long Beach for his phylogenetic analysis of the *rotten ear* gene. The data from these two gentlemen can be found in the results and discussion sections as well as figures 4A-F, 8B-C, and 11-C. I thank you both immensely for contributing to this project.

APPENDIX A: FIGURES AND FIGURE LEGENDS

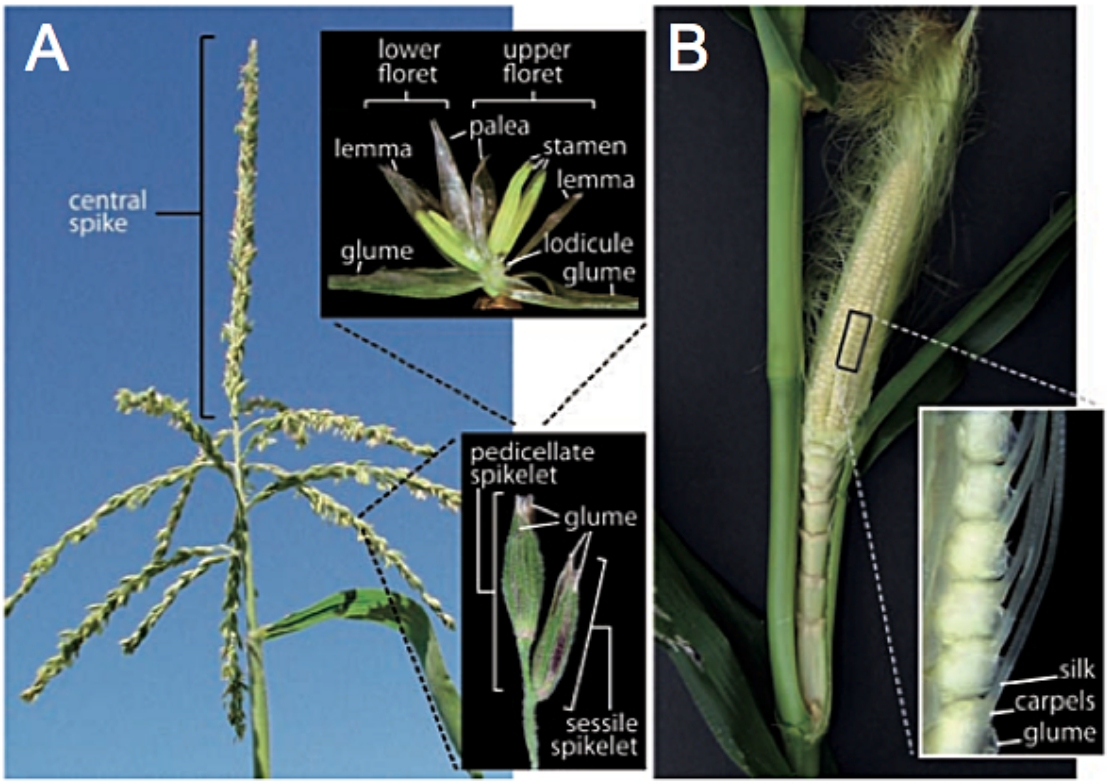

Figure 1. Basic morphology of maize inflorescences.
(A) Wild type male inflorescence (tassel) depicting the central spike and primary branches. Structure of spikelet pair (lower) in addition to inner structure of a tassel spikelet (upper) depicted in inserts. (B) Wild type female inflorescence (ear). Ear spikelet depicted in insert. Lemma, palea, and lodicules of female spikelet covered by glume. (from Vollbrecht and Schmidt, 2009).

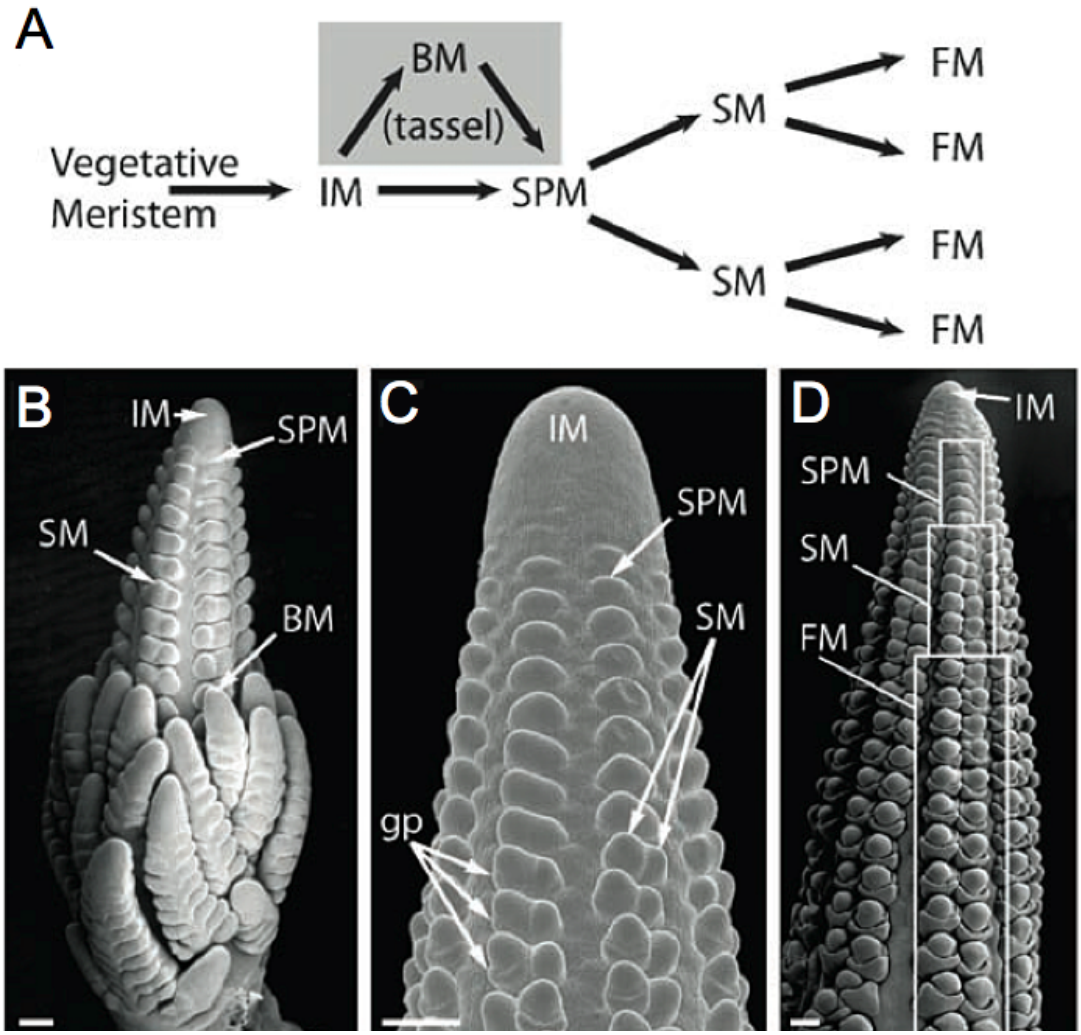

Figure 2. Meristem identity development of male and female inflorescences
(A) Basic schematic outlining the progression of meristem identity. (B-D) SEM micrographs of young tassel and ear, indicating the different types of meristem tissue. (B,C) Young tassel primordia (D) Young ear primordia. (IM) Inflorescence meristem; (SPM) Spikelet pair meristem; (SP) Spikelet meristem; (FM) Floral meristem, (gp) Glume primordia. (from Vollbrecht and Schmidt, 2009)

Scale bars in (B-D) indicate 200 μm.

Figure 3. Ear phenotype of the *rte* mutant.
(A) Unfertilized wild-type ear. Ear phenotypes in *rte-2* (B; mild allele) and in *rte-1* plants (C,D; strong allele).

Scale bar in (A) indicates 2 cm in all panels.

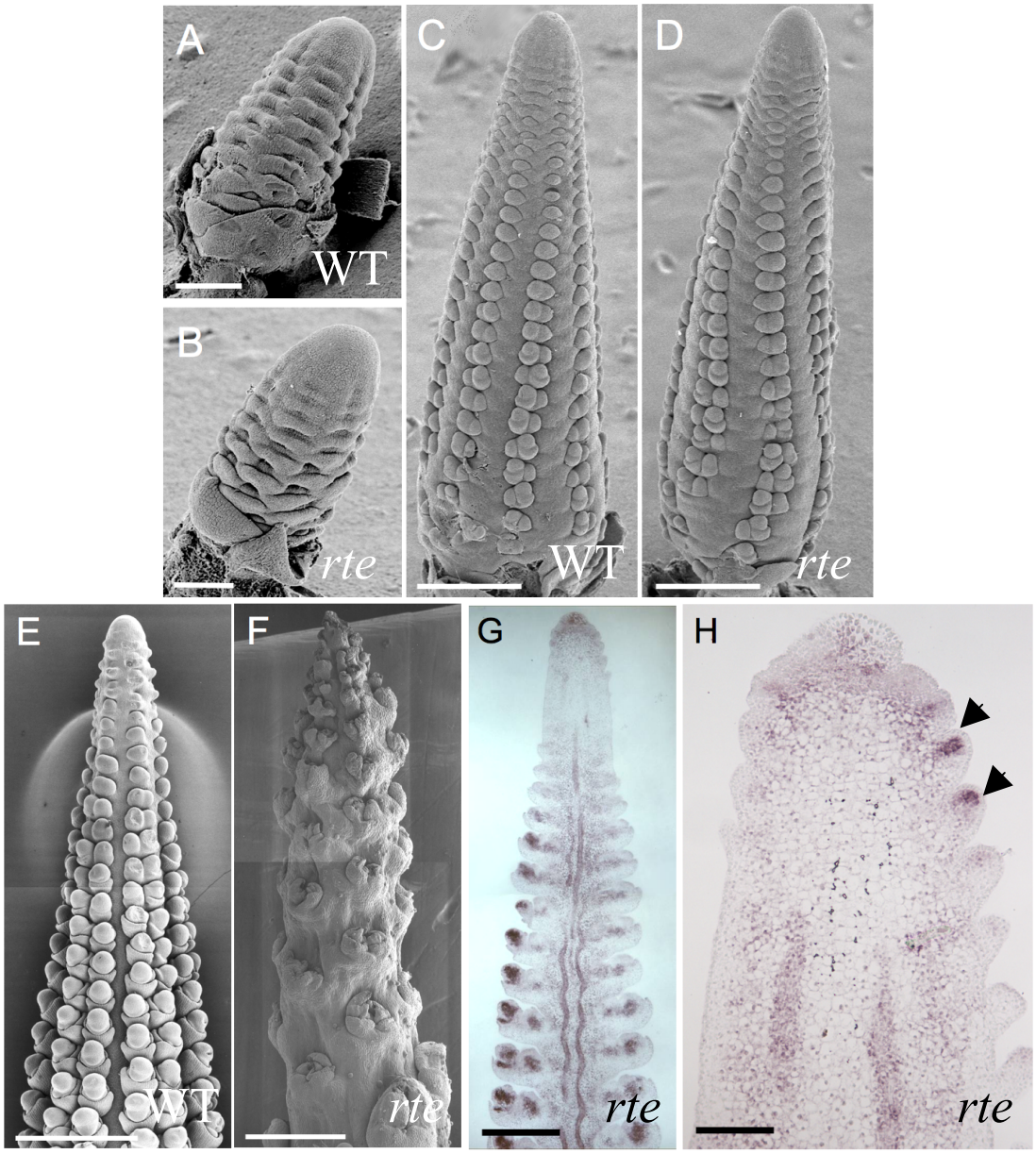

Figure 4. Analysis of *rte* ear primordia.
SEM micrographs of early stage wild-type (A) and *rte* (B) ear primordium. SEM micrographs of wild type (C) and *rte* (D) ears at a subsequent level of development. SEM micrographs of wild-type (E) and *rte* (F) ear tip phenotypes at an advanced stage of development. (G, H) *In situ* hybridization of 0.5 cm *rte* ear tip with *Kn1* probe. (H) depicts detail of *rte* ear tip. Spikelet pair meristems indicated with arrows.

Scale bars in (A), (B), (G) and (H) indicate 200 µm. Scale bars in (C) and (D) indicate 500 µm, and scale bars in (E) and (F) indicate 720 µm.

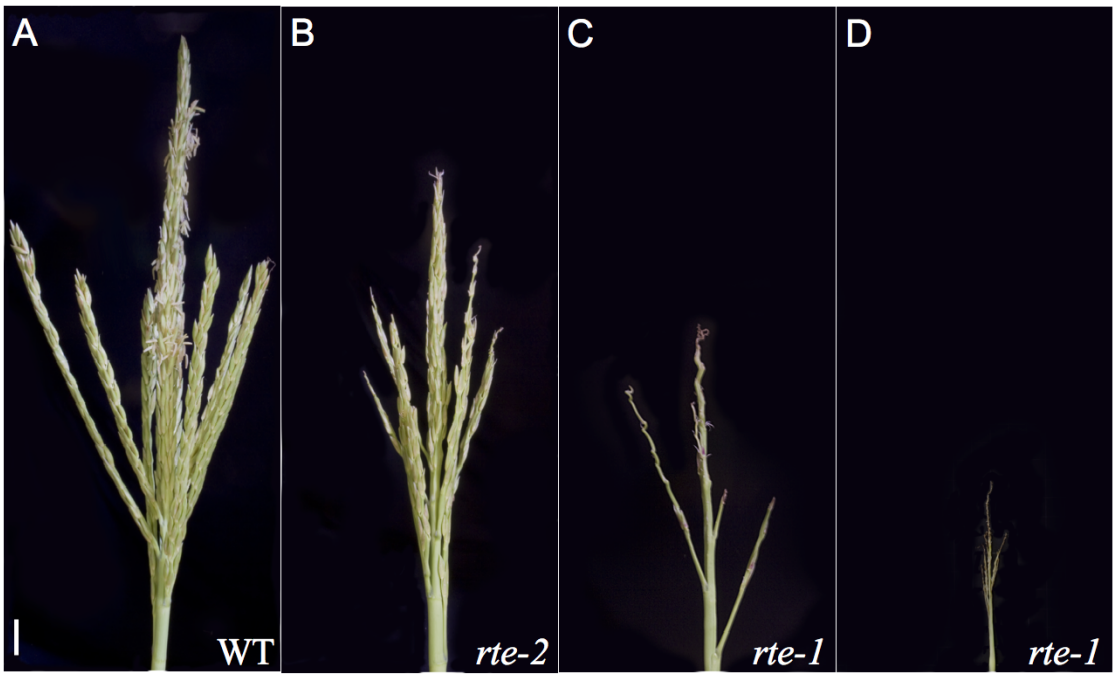

Figure 5. Tassel phenotype of the *rte* mutant.
(A) Wild-type tassel. Tassel phenotypes in *rte-2* (B; mild allele) and in *rte-1* plants (C,D; strong allele).

Scale bar in (A) indicates 2 cm in all panels.

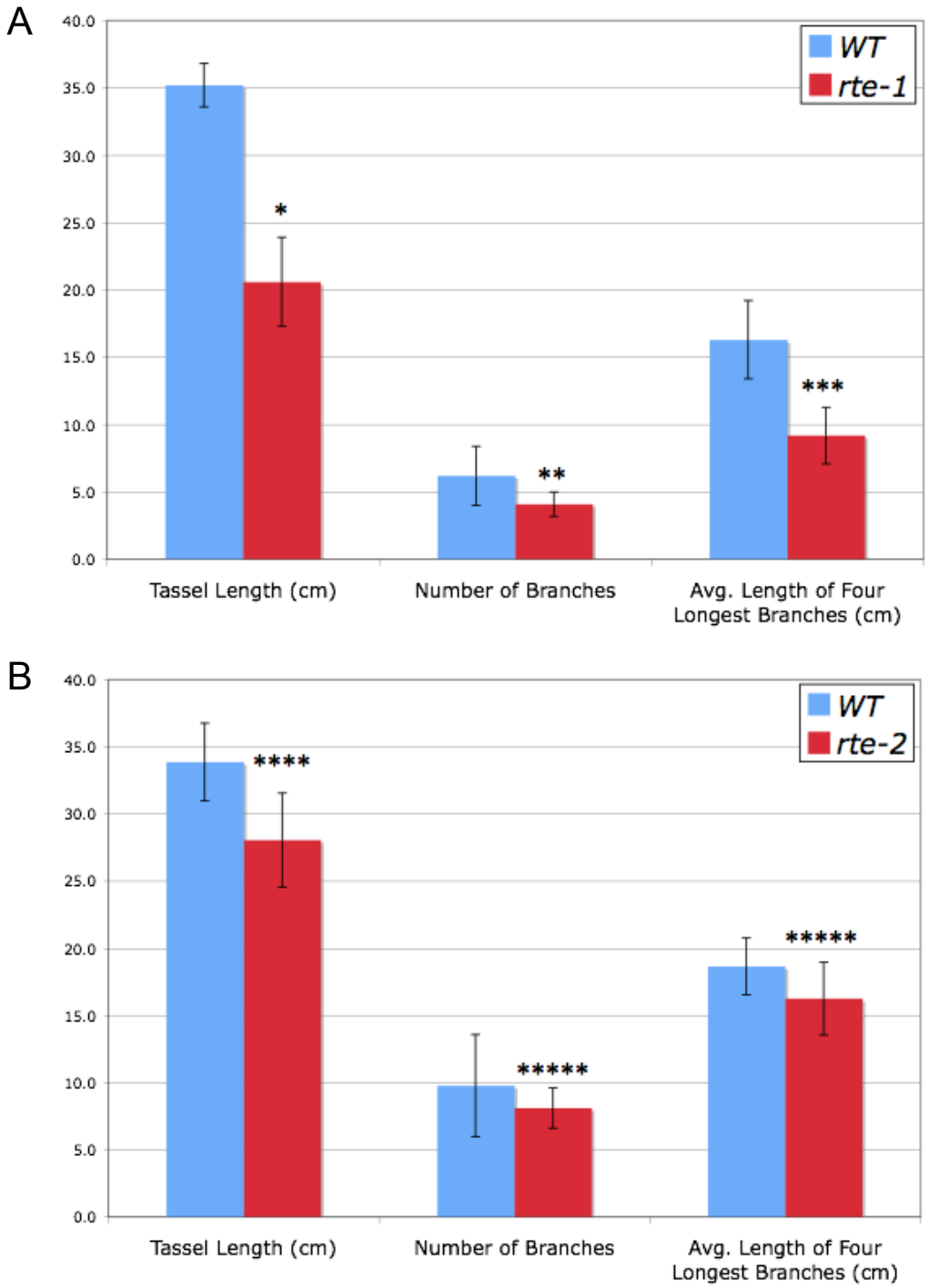

Figure 6. Quantitative phenotypic analysis of wild-type and *rte* tassels. Comparisons of tassel length and branch length and number between wild-type and *rte-1* (A) and *rte-2* (B) alleles, respectively. **t* test, P = <0.0001; ***t* test, P = 0.016; ****t* test, P = 0.0450; *****t* test, P = 0.0015; ******t* test, P = 0.2

(n = 9 for both populations)

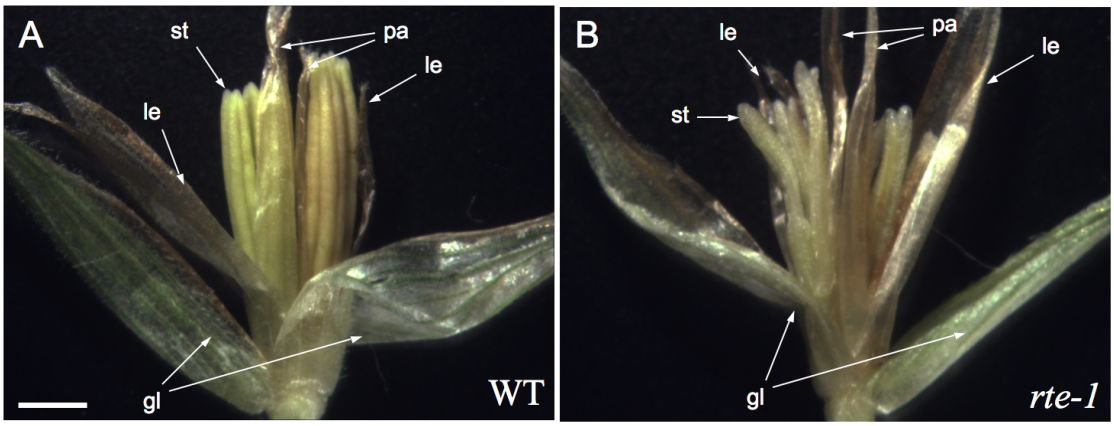

Figure 7. Spikelet comparison of wild-type and *rte* mutant.
(A) Wild-type spikelet, dissected to view inner structure. (B) *rte* mutant spikelet (*rte-1*). The pollen amount in *rte* stamens is drastically reduced. (gl) Glume; (le) Lemma; (pa) Palea; (st) Stamen. Lodicule is present but obscured.

Scale bar in (A) indicates 1 mm.

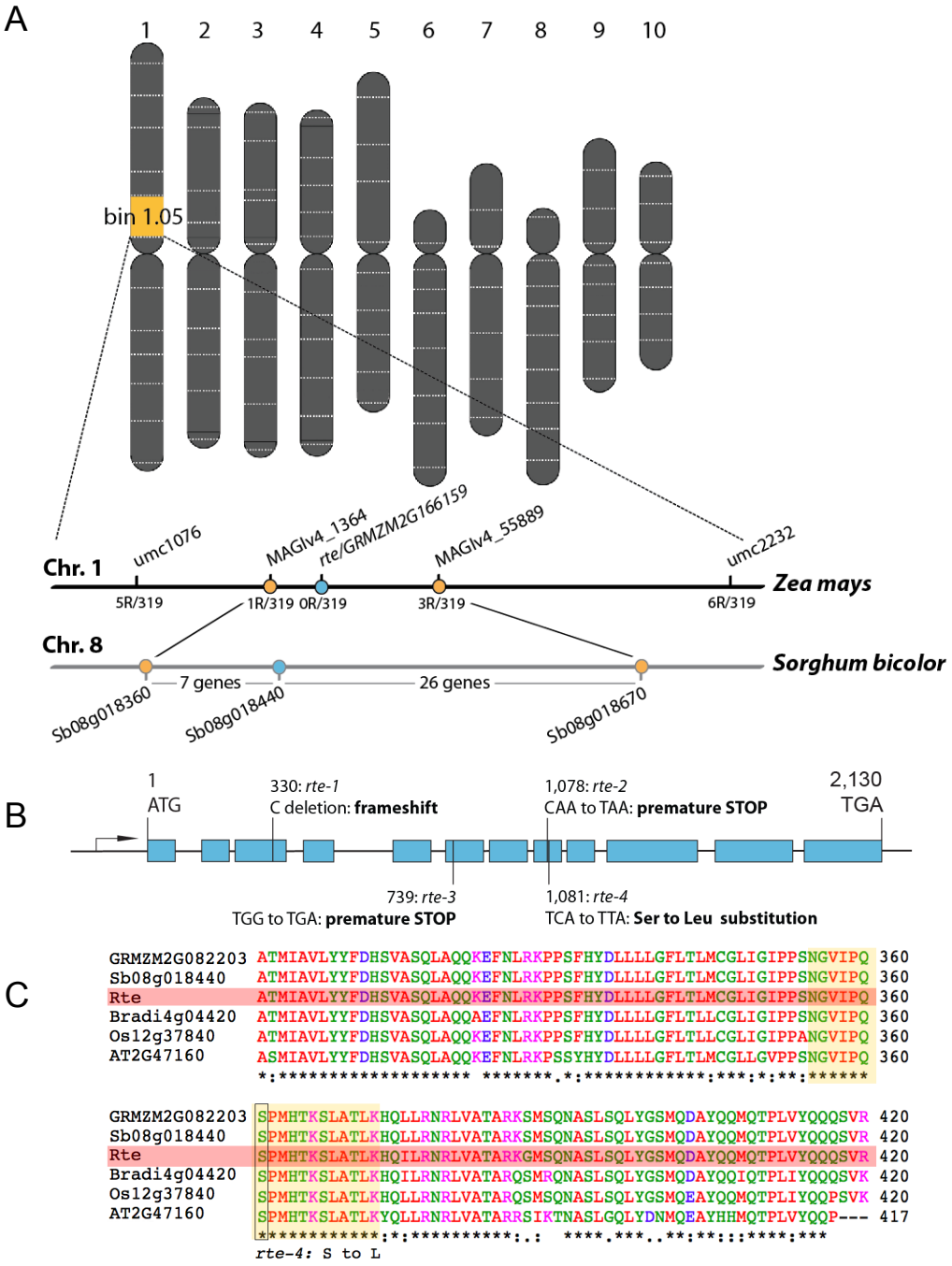

Figure 8. Positional cloning of the *Rte* gene.
(A) Top, a graphical representation of the 10 chromosomes in *Zea mays*. Highlighted in yellow, the genomic region in which the *Rte* gene is located (chromosome 1). Below, the syntenic region in *Sorghum bicolor* (grey) used to search for candidate genes. (B) Representation of the *Rte* gene. The exons are represented as solid blue boxes. The mutations for all of the *rte* alleles identified are also indicated. (C) ClustalW2 amino acid alignment of a conserved segment from *Rte* and *Rte* relatives from other plant species. The *rte-4* mutation created an amino acid change in this conserved region.

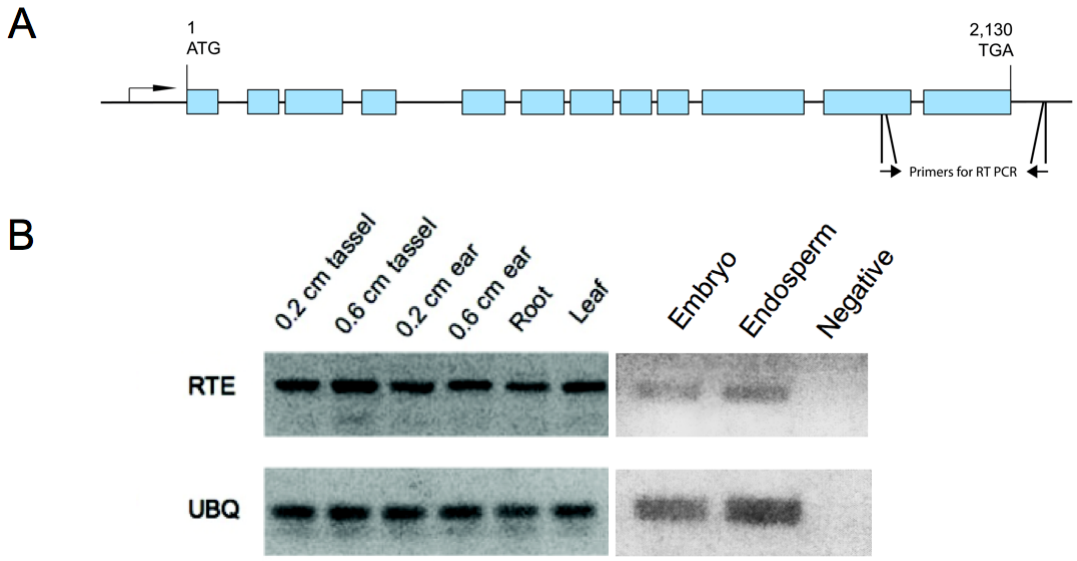

Figure 9. *Rte* RT-PCR expression analysis.
(A) Diagram illustrating the amplicon used for RT-PCR assays. (B) RT-PCR studies of the *Rte* gene in different wild-type tissues. The *Ubiquitin* (*UBQ*) gene was used as control. *Rte* appears to be expressed in both reproductive and vegetative tissue.

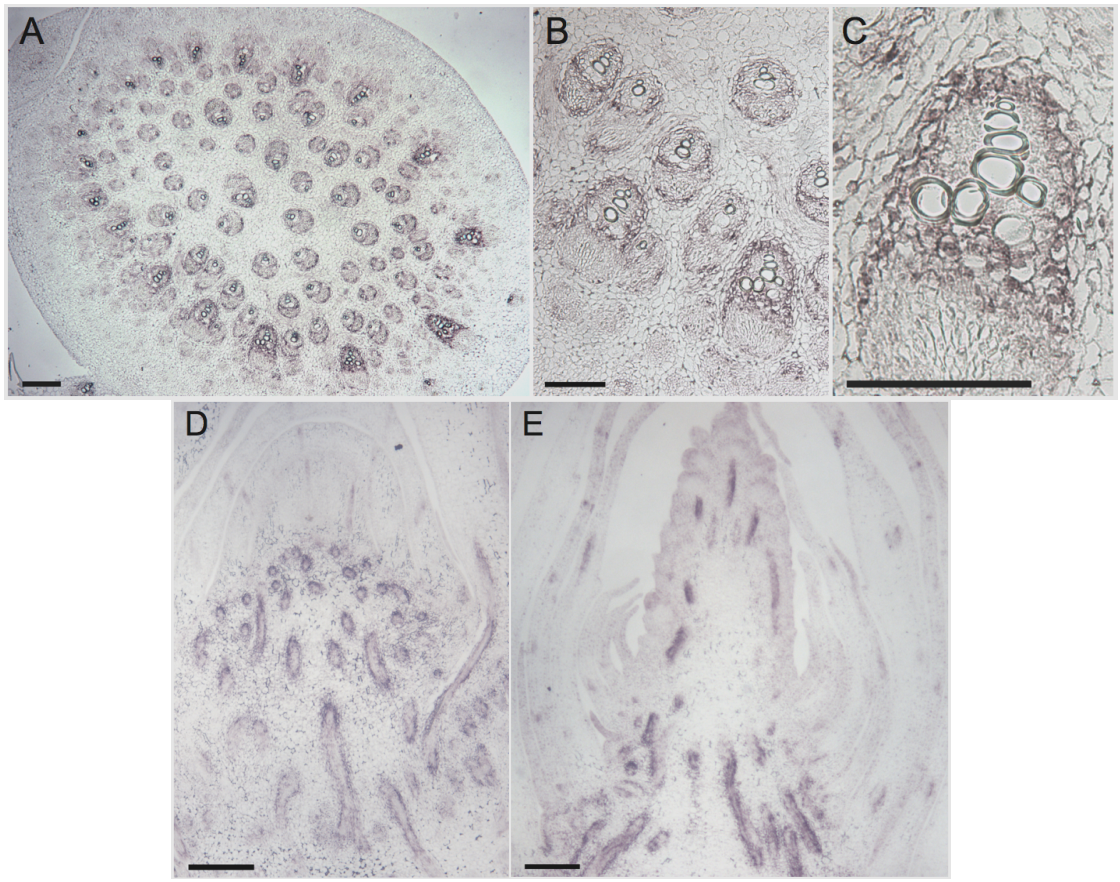

Figure 10. RNA *in situ* localization of *Rte.*
(A-C) Transverse section of young maize seedling. *Rte* expression is present in vascular tissue, mainly surrounding the xylem. (D and E) Localization of *Rte* in longitudinal sections of immature ears. *Rte* messenger RNA is mainly detected in the vasculature.

Scale bars in (A-E) indicate 0.2 mm.

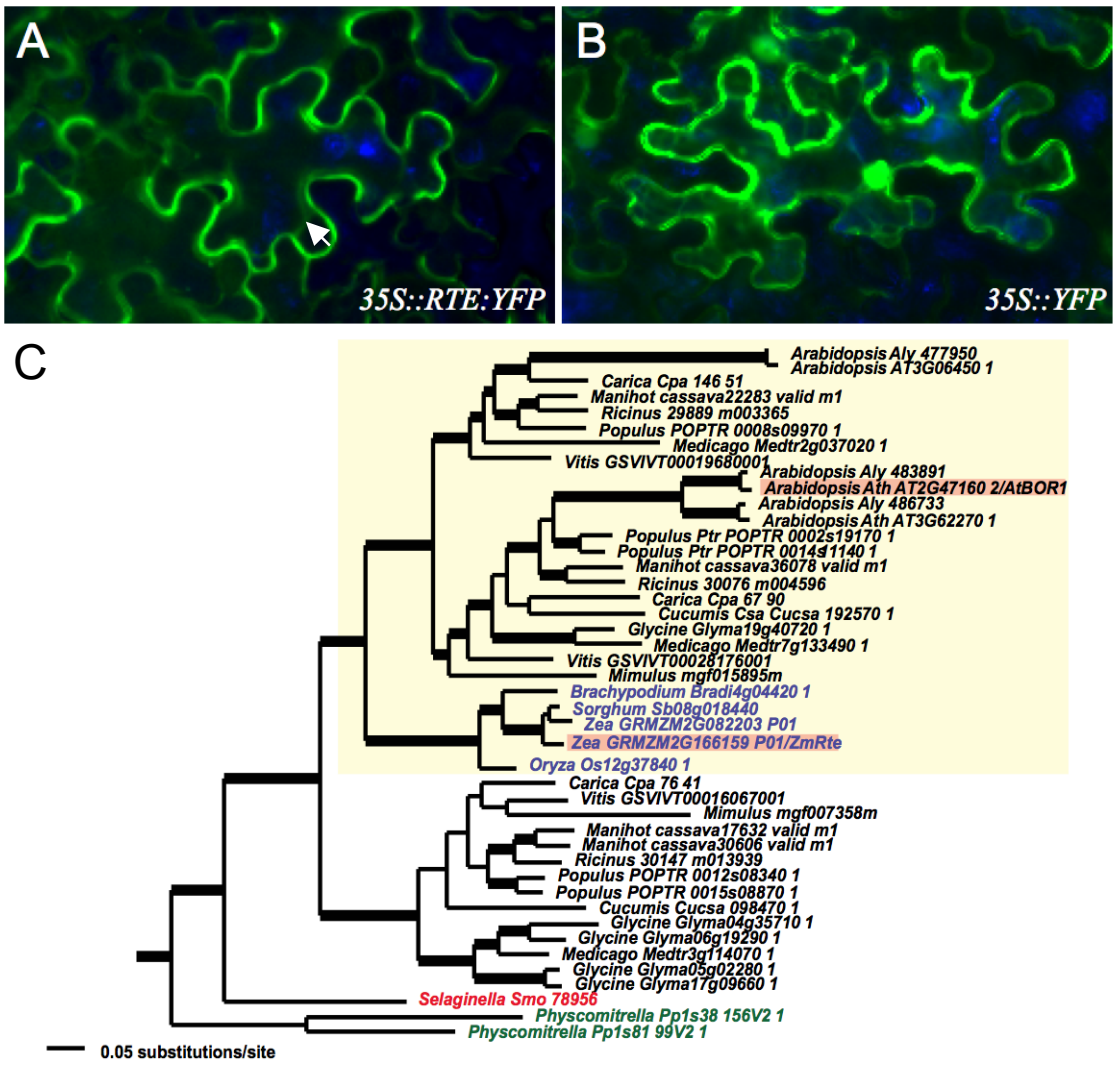

Figure 11. Transient assays using *Nicotiana* leaves to study the subcellular localization of RTE and Phylogenetic analysis of *Rte.*

(A) The RTE:YFP (*35S::RTE:YFP*) fused protein is mainly localized to the plasma membrane (arrows indicate some tonoplast localization), whereas the YFP control (*35S::YFP*) is more homogeneously distributed (B). (C) Bayesian tree of 44 *Rte* relatives. *Rte* and the *Arabidopsis BOR1* (highlighted in red) are shown to share a clade with other similar genes (yellow). Additionally, within this clade *Rte* shares a subclade with other monocot species (blue text). Bold branches supported by ≥0.95 posterior probability.

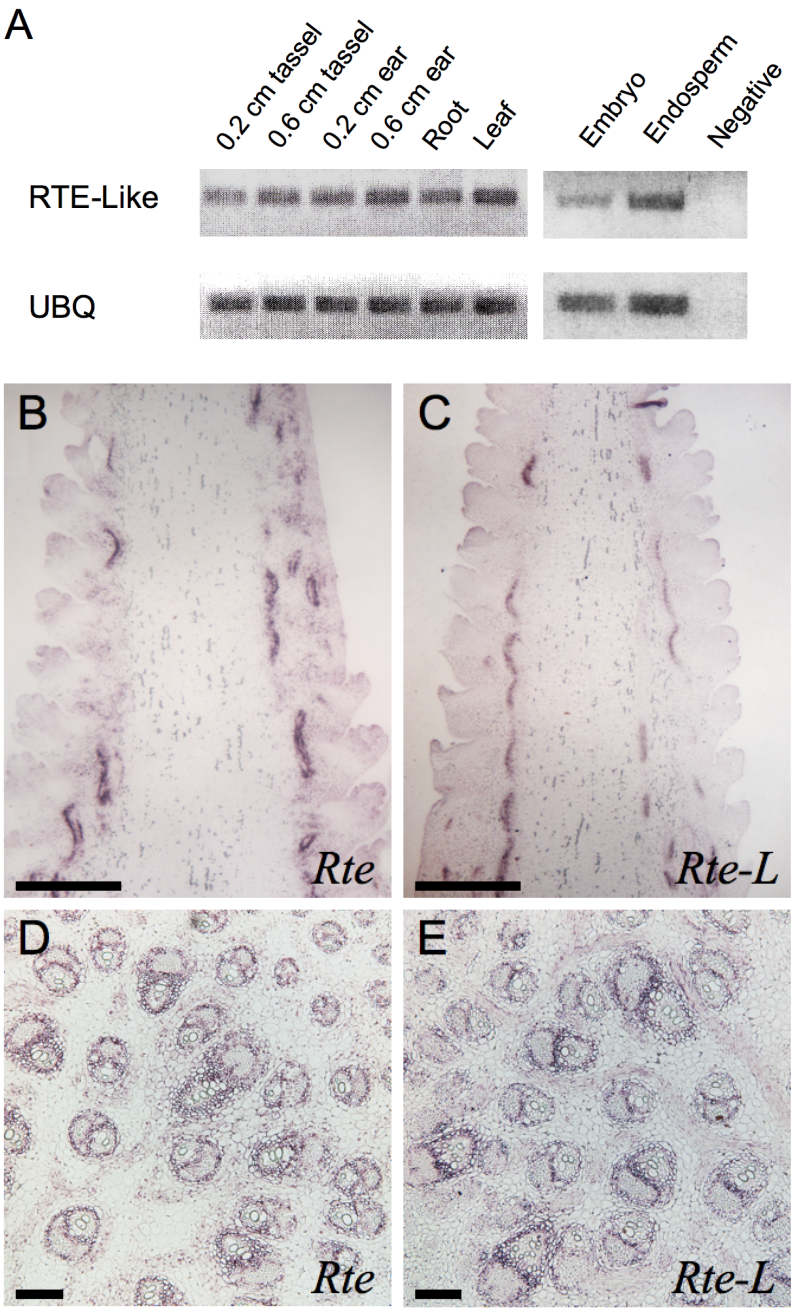

Figure 12. **Expression analysis of the *Rte* paralog (*Rte-Like*).**
(A) RT-PCR studies of the *Rte-Like* gene in different wild-type tissues. The *Ubiquitin* (*UBQ*) gene was used as control. Similar to *Rte, Rte-Like* appears to be expressed in both reproductive and vegetative tissue. (B-E) RNA *in situ* hybridizations of *Rte* and *Rte-L*. (B, C) Localization of mRNA in longitudinal sections of immature ears. (D, E) Transverse section of young maize seedling, focusing on vasculature.

Scale bars in (B, C) indicate 0.5 mm. Scale bars in (D, E) represent 0.2 mm.

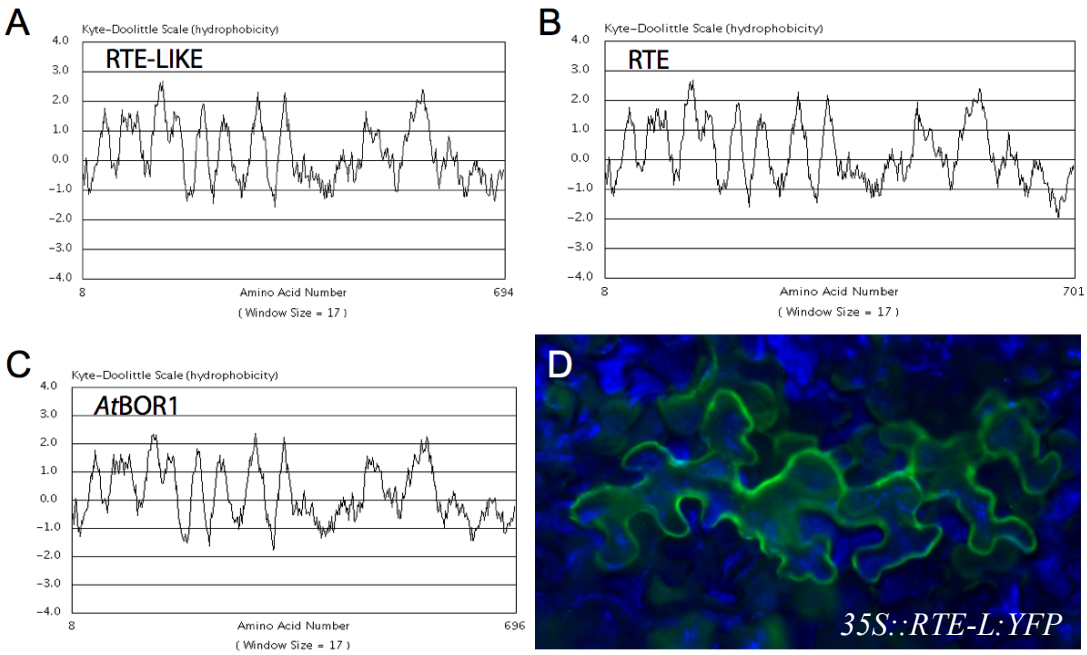

Figure 13. Hydropathy plots and protein localization of RTE-L.
Hydropathy plots of amino acid sequences, generated as described by Kyte and Doolittle: (A) RTE-LIKE (B) RTE (C) *At*BOR1. (D) Transient expression assays in *Nicotiana* leaves show the RTE-L:YFP (*35S::RTE-L:YFP*) fused protein localized mainly to the plasma membrane.

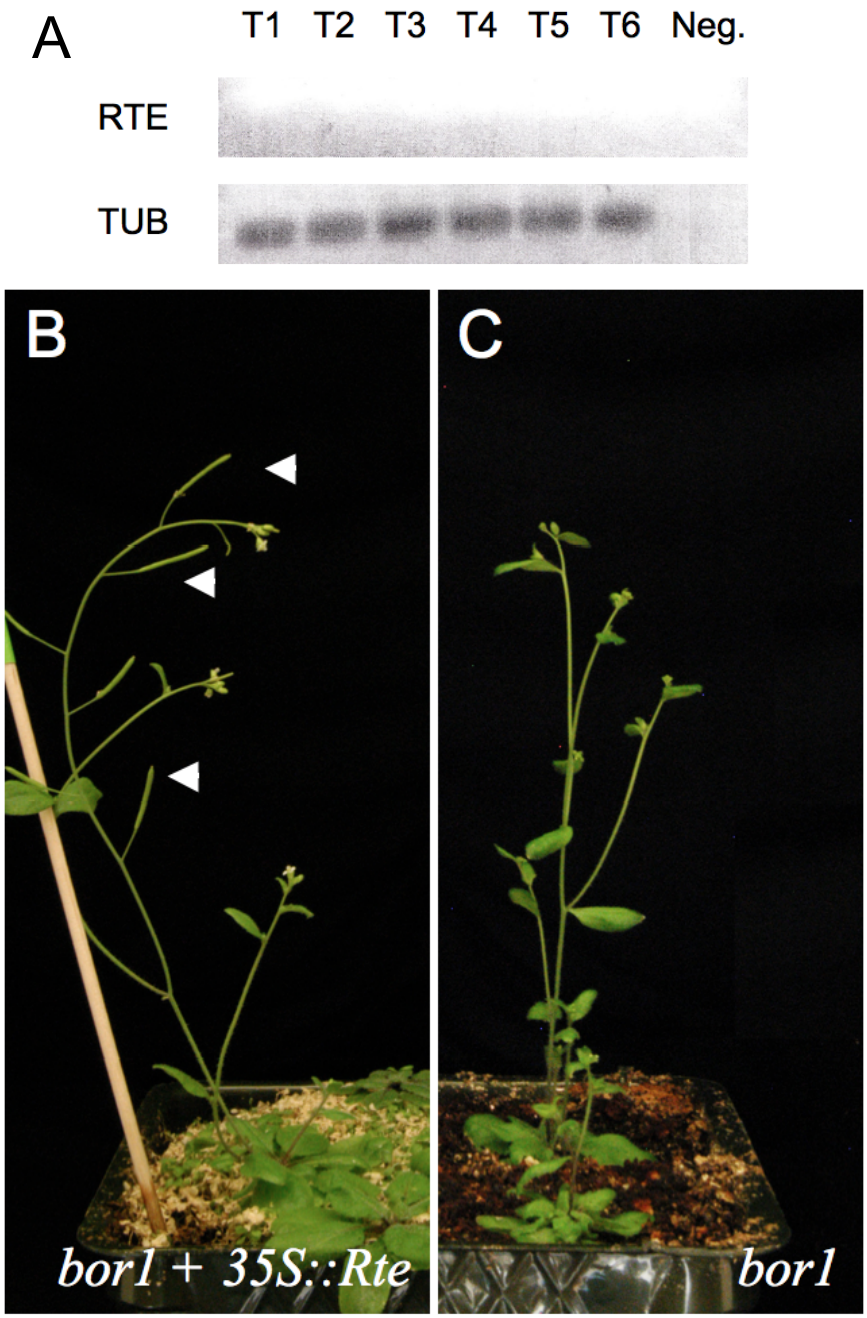

Figure 14. Genetic complementation of *Arabidopsis bor1* with *Rte*.
(A) Detection of *Rte* mRNA in initial *Arabidopsis* transformants of *pBOR1::Rte* using RT-PCR. No *Rte* expression is observed. *Tubulin* (*TUB*) was used as a control. (B) *bor1* mutant transformed with *35S::Rte* construct. Arrows indicate developing fruit. (C) Untransformed *bor1* mutant.

APPENDIX B: TABLES AND TABLE LEGENDS

Table 1. Mutants mapped by Bulk Segregant Analysis.
List of the maize mutant populations that I was personally involved in mapping. Included is a brief description of the mutant phenotype, as well as the status of the mutant mapping.

Mutant	Description	Status
WL-SLO164	BLEACHED DEAD	Confirmed, bin 5.08
04HI-A632XOH43GN-225	SMALL PLANT	BSA Not Confirmed
04HI-Mo17XA632GN-157a	ADHERENT	Confirmed bin 1.08
04MO-A619XB73GN-328	ADHERENT	Confirmed bin 7.02
04HI-A632XOH43GN-105	BARREN	Allelic, *barren inflorescence2* (McSteen and Hake, 2001)
03IL-A619TR-358	UNBRANCHED	Allelic, *liguleless2* (Walsh et al., 1999)
04HI-A632XOH43GN-341	UPRIGHT TASSEL	Allelic, *ramosa enhancer locus2* (Gallavotti et al., 2010)
03HI-B73GN-203	EARLESS	Allelic, *ramosa enhancer locus2* (Gallavotti et al., 2010)
04HI-A632XOH43GN-225	SMALL, STRIPED LEAVES	Confirmed, bin 7.03
TSH ra2EMS	TASSEL SHEATH	Confirmed, bin 6.06
04Mo-A619XB73GN-114	EARLESS	BSA Failed
03HI-B73xMo17GN-528	SMALL, STRIPED LEAVES	Confirmed, bin 6.07
03HI-B73XMo17GN-767	BLASTED	BSA Not Confirmed
03HI-B73XMo17GN-1165	BLASTED	Confirmed, bin 4.09
03IL-A619TR-169	UNBRANCHED	BSA Not Confirmed
04HI-Mo17XA632GN-157b	ROTTEN EAR	Confirmed, bin 1.05
04HI-Mo17XA632GN-16	ROTTEN EAR	Cloned, *Rotten Ear*
04HI-Mo17xA632GN-128	ROTTEN EAR	Cloned, *Rotten Ear*
04HI-OH43xA632GN-190	ROTTEN EAR	Cloned, *Rotten Ear*

Table 2. Markers used for mapping the *rte* mutation.
The following markers and their accompanying oligonucleotides were used to positionally clone the *rte* mutation. All markers are located on Chromosome 1, bins 1.05 and 1.06.

Marker	Contig	BAC	Mb	Forward and Reverse Primers (5' → 3')
umc1515	26	c0455F17	100.0	F: AGAGAGGCTGCTTCAATAAGTTGC R: TTAGTAGTTTCGGTGTCCGTTTCC
umc1493	29	c0226C16	121.9	F: CAACATTTTCCTCAAAACAGACACA R: CAGAAATTTTTGCCTTGGAGTTGT
umc1461	29	c0226C16	122.1	F: GGTCACTTCTTGCACCTTTCTGAG R: GTCTTTGGGTTGTGATCCCCTT
umc1076	30	c0326E07	143.5	F: TTGGAAATCACCAATTGATATAGTTTG R: TCTATTGCAAACGCCAAAAGTAGC
RE-T13 (MAGIv4_1364)	31	c0114A19	148.5	F: GTTGACATCTCTACTACTAAGGTC R: AGCCTGGAGAAGATATGGACGACT
RE-T12-AluI (MAGIv4_55889) [dCAPS]	31	c0277F10	151.7	F: AGCAGCCTGCCTTATCTTCACAGC R: CTGATGTCAGGCTTGCAGCTACAC
umc2232	33	b0293M22	164.5	F: CTAGATTGCCTCGGACCTGTAAGA R: CATTCATCCACCATAAATATCCTGC
umc1508	37	b0057L06	183.8	F: GGTTCTTGGTTTGGGCCTTAGTAT R: GAGGCCACTAGTTGACCTTTTTCA
bnlg1057	38	b0232P19	191.0	F: TTCACCGCCTCACATGAC R: GCAACGCTAGCTAGCTTTG
bnlg1615	40	c0529J23	192.9	F: CAGAAGGGGAGGAGGGATAC R: ATTATGCTCAAGCACAGGGC
umc1035	41	c0157N16	195.6	F: CTGGCATGATCACGCTATGTATG R: TAACATCAGCAGGTTTGCTCATTC

Table 3. Oligonucleotides used for sequencing of the *Rte* gene candidate.
The following oligonucleotides were used to amplify three fragments of the *Rte* candidate gene, in order to detect lesions in the coding sequence.

Primer Name		Primer Sequence (5' → 3')
Fragment 1	RE-T25-F1	CCGACTGGCCATCCAGAATATACC
	RE-T25-R1	GCACATGCCTTTGAGCAACCTACT
Fragment 2	RE-T25-F2	CTCTGTGGCCATCTGGATGTGCGA
	RE-T25-R2	TGCCATGTGAGTGAGAAATCAGATG
Fragment 3	RE-T25-F3	CATCTGATTTCTCACTCACATGGCA
	RE-T25-R3	GGAGTGCTATACCTGTAATCTCTG

Table 4. Primers used for genotyping the *rte* mutants.
The following primers were used to genotype plants for the *rte-1* and *rte-2* alleles. Indicated are the restriction enzymes needed to detect the polymorphisms between the wild-type and mutant sequence. Bold letters indicate base pair change from genomic sequence.

Primer Name		Primer Sequence (5' → 3')	Bands
rte-1 [CAPS]	RE-StyI F2	TACTTGTGCAGATGGAGTCCTCAC	Wild-Type: 168 & 153 bp fragments Mutant: 321 bp
	RE-T25-R10	CTGCACGCAAACATGACAACAAC	
rte-2 [dCAPS]	RE-RsaI-F	CCTCCATCAAATGGTGTCATT**GT**A	Wild-Type: 263 bp fragment Mutant: 285 bp
	RE-T25-R4	CTCTTCTGACAGACTGTTGCTGAT	

Table 5. Oligonucleotides used for isolating the *Rte* and *Rte-L* coding sequence. The following oligonucleotides were used to amplify the complete *Rte* and *Rte-L* wild-type coding sequence using RT-PCR.

Primer Name			Primer Sequence (5' → 3')
Rte	Fragment 1	RE-cds-F1	ATGGAGGAGAGCTTCGTGCCCTTG
		RE-cds-R3	CACCATCGAAGCCTGTAGAAGGTTG
	Fragment 2	RE-cds-F3	ACAGGCTTCGATGGTGGTGGGCTGT
		RE-cds-R2	TCACTTTGGTGCCGAGCCTTCACC
Rte-L	Fragment 1	RE-cds-F1	ATGGAGGAGAGCTTCGTGCCCTTG
		RE-cds-R1	CACCATGGAAGCCTGTAGCAAGTTG
	Fragment 2	RE-cds-F2	ACAGGCTTCCATGGTGGGTGGTTGT
		RE-cds-R2	TCACTTTGGTGTTGAGCCTTCACC

Table 6. Oligonucleotides used for Reverse Transcriptase (RT) PCR.
The following oligonucleotides were used to detect levels of mature *Rte* and *Rte-L* mRNA from different types of maize tissue from the B73 inbred line by RT-PCR. *Ubiquitin* (*UBQ*) was used as a control.

Primer Name	Primer Sequence (5' → 3')
RE-T25-F7	CAGGCAGTACATCCTCCCTAAGCTC
RE-T25-R6	TCTCATCAGAGGACATCTTGGA
RteL-RTPCR-F1	CCCAAGCTCTTCAAAGGTGCGCA
RteL-RTPCR-R1	AACTGATGACCAGTGGTTGAATAGC
UBQ-F	TAAGCTGCCGATGTGCCTGCGTCG
UBQ-R	CTGAAAGACAGAACATAATGAGCACAG

Table 7. Oligonucleotides used for *in-situ* probe synthesis.
The following oligonucleotides were used to amplify the *Rte* and *Rte-L* coding sequence for cloning into pAD-GAL4 2.1 cut with *Eco*RI and *Sal*I. The constructs were then used as templates to synthesize antisense mRNA probe for non-radioactive *in situ* hybridization.

Primer Name	Primer Sequence (5' → 3')
RTE-pAD-EcoRI-F1	GGATCCTCTGCTAGCAGAGAATTCATGGAGGAGAGCTTCGTGCC
RTE-pAD-SalI-R2	TCACTATAGGGCTCTAGAGTCGACTCACTTTGGTGCCGAGCCTT
RteL-pAD-EcoRI-F1	GGATCCTCTGCTAGCAGAGAATTCATGGAGGAGAGCTTCGTGCC
RteL-pAD-SalI-R2	TCACTATAGGGCTCTAGAGTCGACTCACTTTGGTGTTGAGCCTT

Table 8. Oligonucleotides used for creation of transient expression constructs. The following oligonucleotides were used to amplify the *Rte, Rte-L* and *YFP* coding sequences for cloning into pBj3635S+2x35S cut with *Xho*I. Prior to cloning, *the Rte* and *Rte-L* coding sequences were each fused together to *YFP*, with *YFP* attached to the C terminal of the *Rte* coding sequence.

Primer Name		Primer Sequence (5' → 3')
Rte Coding Sequence	RTE-35s/pBJ36-XhoI-F1	GTCGACCTGCAGACGCGTCTCGA-GATGGAGGAGAGCTTCGTGCC
	RTE/YFP-R2	CGCCCTTGCTCACCATCTTTGGTGCCGAGCCTT
Rte-L Coding Sequence	RteL-35s/pBJ36-XhoI-F1	GTCGACCTGCAGACGCGTCTCGAG-ATGGAGGAGAGCTTCGTGCCCTTG
	RteL/YFP-R1	CTCCTCGCCCTTGCTCACCATCTT-TGGTGTTGAGCCTTCACC
YFP Coding Sequence	YFP/RTE-F2	AGGCTCGGCACCAAAGATGGTGAGCAAGGGCGA
	YFP-35s/pBJ36-XhoI-R1	ACCCGGGGTACCGAATTCCTCGA-GCTAGGCCCCAGCGGCAGCAG

Table 9. Oligonucleotides for creation of constructs for *Arabidopsis* transformation.

The following oligonucleotides were used to amplify the *Rte* coding sequence and *BOR1* native promoter region for cloning into pBj3635S+2XYPetM+3xHA cut with *Xho*I and *Xba*I. Prior to cloning, the two sequences were fused together, with the *BOR1* promoter attached to the N terminal of the *Rte* coding sequence. For creation of the *35S::Rte* construct, the *Rte* coding sequence was amplified with a different set of primers, for cloning into pBJ36+2x35s cut with *Xho*I

Primer Name		Primer Sequence (5' → 3')
BOR1 Promoter Region	BOR1-RTE-3xHA/pBJ36-XhoI-F1	GTCGACCTGCAGACGCGTCTCGAGTAG-TAAAACGAAAATGATAAGAG
	BOR1/RTE-R1	CGAAGCTCTCCTCCATGACTCTGTTTTCTCTCA
Rte Coding Sequence 1	RTE/BOR1-F1	TGAGAGAAAACAGAGTCATGGAGGAGAGCTTCG
	RTE-3xHA/pBJ36-XbaI-R1	GCAGCAGCAGCAGGCAAGTCTAGACC-CTTTGGTGCCGAGCCTT
Rte Coding Sequence 2	RTE-35s/pBJ36-XhoI-F1	GTCGACCTGCAGACGCGTCTCGAGATG-GAGGAGAGCTTCGTGCC
	RTE-35s/pBJ36-XhoI-R1	ACCCGGGGTACCGAATTCCTCGAGTCA-CTTTGGTGCCGAGCCTT

Table 10. Oligonucleotides used for RT-PCR of *pBOR1::Rte Arabidopsis* transformants.

The following oligonucleotides were used to detect levels of mature *Rte* mRNA from *bor1* mutants transformed with the *pBOR1::Rte* construct. ß-*Tubulin* (*TUB*) mRNA was also detected as a control.

Primer Name	Primer Sequence (5' → 3')
Rte-cds-F3	ACAGGCTTCGATGGTGGTGGGCTGT
Rte-cds-R2	TCACTTTGGTGCCGAGCCTTCACC
TUB+	ATGTTCAGGCGCAAGGCTT
TUB-	TCTGCAACCGGGTCATTCAT

Table 11. Oligonucleotides used for genotyping *bor1* mutants.
The following primers were used to genotype *Arabidopsis bor1* mutant transformants and controls to verify T-DNA insertion. A band detected using 037312-F and LBb 1.3 but not using 037312-F and 037312-R indicates a T-DNA insertion mutant.

Primer Name	Primer Sequence (5' → 3')
037312-F	ATGCTTGATGTTCCAATCGTC
037312-R	ATCCATGTGAGACCAAAGCAG
LBb1.3	ATTTTGCCGATTTCGGAAC

Table 12. Quantitative Tassel Analysis
Tassel measurements of wild type and *rte-1* and *rte-2* mutants backcrossed to the Mo17 and A619 backgrounds respectfully. Average numbers are given with standard deviations in parentheses. **t* test, P = <0.0001; ***t* test, P = 0.016; ****t* test, P = 0.0450; *****t* test, P = 0.0015; ******t* test, P = 0.2

Phenotype	*n*	Tassel Length (cm)	Number of Primary Branches	Branch Length (cm)
Wild Type	9	35.2 (1.6)	6.2 (2.2)	16.3 (2.9)
rte-1	9	20.6 (3.3)*	4.1 (0.9)**	9.2 (2.1)***
Wild Type	9	33.9 (2.9)	9.8 (3.8)	18.7 (2.1)
rte-2	9	28.1 (3.5)****	8.1 (1.5)*****	16.3 (2.7)*****

REFERENCES

Agarwala, S., Sharma, P., Chatterjee, C., and Sharma, C. (1981). Development and enzymatic changes during pollen development in boron deficient maize plants. J. Plant Nutr. *3,* 329-336.

Alonso, J.M., Stepanova, A.N., Leisse, T.J., Kim, C.J., Chen, H., Shinn, P., Stevenson, D.K., Zimmerman, J., Barajas, P., Cheuk, R*., et al.* (2003). Genome-Wide Insertional Mutagenesis of Arabidopsis thaliana. Science *301,* 653-657.

Argust, P. (1998). Distribution of boron in the environment. Biol Trace Elem Res *66,* 131-143.

Bennetzen, J., and Hake, S. (2009). Handbook of Maize: Its Biology (New York, New York: Springer).

Bienert, G.P., Schüssler, M.D., and Jahn, T.P. (2008). Metalloids: essential, beneficial or toxic? Major intrinsic proteins sort it out. Trends Biochem Sci. *33,* 20-26.

Cheng, P.C., Greyson, R.I., and Walden, D.B. (1983). Organ Initiation and the Development of Unisexual Flowers in the Tassel and Ear of *Zea mays*. Am. J. Bot *3,* 450-462.

Clough, S.J., and Bent, A.F. (1998). Floral dip: a simplified method for Agrobacterium-mediated transformation of *Arabidopsis thaliana*. Plant J. *16,* 735-743.

Dell, B., and Huang, L. (1997). Physiological response of plants to low boron. Plant and Soil *193,* 103-120.

Edgar, R. (2004). MUSCLE: a multiple sequence alignment method with reduced time and space complexity. BMC Bioinf. *5,* 113.

Findeklee, P., and Goldbach, H.E. (1996). Rapid Effects of Boron deficiency on cell wall elasticity modulus in *Cucurbita pepo* roots. Bot. Acta. *109,* 463-465.

Fleischer, A., O'Neil, M.A., and Ehwald, R. (1999). The pore size of non-graminaceaous plant cell walls is rapidly decreased by borate-ester cross linking of the pectic polysaccharide rhamnogalacturonan II. Plant Physiol. *121,* 829-838.

Gallavotti, A., Barazesh, S., Malcomber, S., Hall, D., Jackson, D., Schmidt, R.J., and McSteen, P. (2008). *sparse inflorescence1* encodes a monocot-specific *YUCCA*-like gene required for vegetative and reproductive development in maize. Proc Natl Acad Sci U S A *105,* 15196-15201.

Gallavotti, A., Zhao, Q., Kyozuka, J., Meeley, R.B., Ritter, M.K., Doebley, J.F., Pe, M.E., and Schmidt, R.J. (2004). The role of *barren stalk1* in the architecture of maize. Nature *432,* 630-635.

Gallavotti, A., Malcomber, S., Gaines, C., Stanfield, S., Whipple, C., Kellogg, E., and Schmidt, R.J. (2011). BARREN STALK FASTIGATE Is an AT-Hook Protein Required for the Formation of Maize Ears. Plant Cell *23,* 1756-1771.

Gallavotti, A., Long, J.A., Stanfield, S., Yang, X., Jackson, D., Vollbrecht, E., and Schmidt, R.J. (2010). The control of axillary meristem fate in the maize *ramosa* pathway. Development 137, 2849-2856.

Gallavotti, A., Yang, Y., Schmidt, R.J., and Jackson, D. (2008). The Relationship between Auxin Transport and Maize Branching. Plant Physiol. *147,* 1913-1923.

Gälweiler, L., Guan, C., Müller, A., Wisman, E., Mendgen, K., Yephremov, A., and Palme, K. (1998). Regulation of Polar Auxin Transport by AtPIN1 in Arabidopsis Vascular Tissue. Science *282,* 2226-2230.

Gaut, B.S., and Doebley, J.F. (1997). DNA sequence evidence for the segmental allotetraploid origin of maize. Proc. Natl. Acad. Sci. U S A *94*, 6809–6814.

Gleave, A.P. (1992). A versatile binary vector system with a T-DNA organisational structure conducive to efficient integration of cloned DNA into the plant genome. Plant Mol Biol *20,* 1203-1207.

Gupta, U.C. (1979). Boron Nutrition of Crops. Adv. Agron. *31,* 273-307.

Huang, L., Pant, J., Dell, B., and Bell, R.W. (1999). Effects of Boron Defciency on Anther Development and Floret Fertility in Wheat (*Triticum aestivum* L. `Wilgoyne'). Ann. Bot. *85,* 493-500.

Kerstetter, R.A., Laudencia-Chingcuanco, D., Smith, L.G., and Hake, S. (1997). Loss-of-function mutations in the maize homeobox gene, *knotted1*, are defective in shoot meristem maintenance. Development *124,* 3045-3054.

Kobayashi, M., Matoh, T., and Azuma, J. (1996). Two Chains of Rhamnogalacturonan II Are Cross-Linked by Borate-Diol Ester Bonds in Higher Plant Cell Walls. Plant Physiol. *110,* 1017-1020.

Kyte, J., and Doolittle, R.F. (1982). A simple method for displaying the hydropathic character of a protein. J. Mol. Biol. *157,* 105-132.

Liu, S., Chen, H.D., Makarevitch, I., Shirmer, R., Emrich, S.J., Dietrich, C.R., Barbazuk, W.B., Springer, N.M., and Schnable, P.S. (January 2010). High-Throughput Genetic Mapping of Mutants via Quantitative Single Nucleotide Polymorphism Typing. Genetics *184,* 19-26.

Lodish, H., Berk, A., Kaiser, C.A., Krieger, M., Scott, M.P., Bretscher, A., Ploegh, H., and Matsudaira, P. (2008). Molecular Cell Biology, Sixth Edition (New York: W. H. Freeman and company).

Loomis, D.W., and Durst, R.W. (1992). Chemistry and biology of boron. BioFactors *3,* 229-239.

McCauley, A., Jones, C., and Jacobsen, J. (2003). Plant Nutrient Functions and Deficiency and Toxicity Symptoms. Retrieved August 23, 2011, from [http://landresources.montana.edu/NM/Modules/Module9.pdf]

McSteen, P., and Leyser, O. (2005). Shoot Branching. Annu Rev Plant Bio *56,* 353-374.

McSteen, P., and Hake, S. (2001). *barren inflorescence2* regulates axillary meristem development in the maize inflorescence. Development 128, 2881-2891.

McSteen, P., Laudencia-Chingcuanco, D., and Colasanti, J. (2000). A floret by any other name: control of meristem identity in maize. Trends Plant Sci. *5,* 61-66.

Miwa, K., Takano, J., and Fujiwara, T. (2006). Improvement of seed yields under boron-limiting conditions through overexpression of *BOR1*, a boron transporter for xylem loading, in Arabidopsis thaliana. Plant J. *46,* 1084-1091.

Nakagawa, Y., Hanaoka, H., Kobayashi, M., Miyoshi, K., Miwa, K., and Fujiwara, T. (2007). Cell-Type Specificity of the Expression of Os *BOR1*, a Rice Efflux Boron Transporter Gene, Is Regulated in Response to Boron Availability for Efficient Boron Uptake and Xylem Loading. Plant Cell *19,* 2624-2635.

Noguchi, K., Yasumori, M., Imai, T., Naito, S., Matsunaga, T., Oda, H., Hayashi, H., Chino, M., and Fujiwara, T. (1997). *bor1-1*, an Arabidopsis thaliana Mutant That Requires a High Level of Boron. Plant Physiol. *115,* 901-906.

Phillips, K.A., Skirpan, A.L., Liu, X., Christensen, A., Slewinski, T.L., Hudson, C., Barazesh, S., Cohen, J.D., Malcomber, S., and McSteen, P. (2011). *Vanishing tassel2* Encodes a Grass-Specific Tryptophan Aminotransferase Required for Vegetative and Reproductive Development in Maize. The Plant Cell Online *23,* 550-566.

Raven, P.H., Evert, R.F., and Eichhorn, S.E. (2005). Biology of Plants, Seventh Edition (New York: W.H. Freeman and Company Publishers).

Ritter, M.K., Padilla, C.M., and Schmidt, R.J. (2002). The maize mutant *barren stalk1* is defective in axillary meristem development. Am. J. Bot. *89,* 203-210.

Ronquist, F., and Huelsenbeck, J.P. (2003). MrBayes 3: Bayesian phylogenetic inference under mixed models. Bioinformatics *19,* 1572-1574.

Schnable, P.S., Ware, D., Fulton, R.S., Stein, J.C., Wei, F., Pasternak, S., Liang, C., Zhang, J., Fulton, L., Graves, T.A.*, et al.* (2009). The B73 Maize Genome: Complexity, Diversity, and Dynamics. Science *326,* 1112-1115.

Shorrocks, V.M. (1997). The Occurrence and Correction of Boron Defficiency. Plant Soil *193,* 121-148.

Skirpan, A., Culler, A.H., Gallavotti, A., Jackson, D., Cohen, J.D., and McSteen, P. (2009). BARREN INFLORESCENCE2 Interaction with ZmPIN1a Suggests a Role in Auxin Transport During Maize Inflorescence Development. Plant Cell Physiol. *50,* 652-657.

Skirpan, A., Wu, X., and McSteen, P. (2008). Genetic and physical interaction suggest that BARREN STALK1 is a target of BARREN INFLORESCENCE2 in maize inflorescence development. Plant J. *55,* 787-797.

Strable, J., and Scanlon, M.J. (2009). Maize (*Zea mays*): A Model Organism for Basic and Applied Research in Plant Biology. Cold Spring Harb Protoc. *10*

Sutton, T., Baumann, U., Hayes, J., Collins, N.C., Shi, B., Schnurbusch, T., Hay, A., Mayo, G., Pallotta, M., Tester, M., and Langridge, P. (2007). Boron-Toxicity Tolerance in Barley Arising from Efflux Transporter Amplification. Science *318,* 1446-1449.

Takano, J., Miwa, K., and Fujiwara, T. (2008). Boron transport mechanisms: collaboration of channels and transporters. Trends Plant Sci. *13,* 451-457.

Takano, J., Noguchi, K., Yasumori, M., Kobayashi, M., Gajdos, Z., Miwa, K., Hayashi, H., Yoneyama, T., and Fujiwara, T. (2002). Arabidopsis boron transporter for xylem loading. Nature *420,* 337-340.

Takano, J., Miwa, K., Yuan, L., von Wirén, N., and Fujiwara, T. (2005). Endocytosis and degradation of BOR1, a boron transporter of Arabidopsis thaliana, regulated by boron availability. Proc Natl Acad Sci U S A *102,* 12276-12281.

Takano, J., Wada, M., Ludewig, U., Schaaf, G., von Wirén, N., and Fujiwara, T. (2006). The Arabidopsis Major Intrinsic Protein NIP5;1 Is Essential for Efficient Boron Uptake and Plant Development under Boron Limitation. The Plant Cell Online *18,* 1498-1509.

Tanaka, M., Wallace, I.S., Takano, J., Roberts, D.M., and Fujiwara, T. (2008). NIP6;1 Is a Boric Acid Channel for Preferential Transport of Boron to Growing Shoot Tissues in Arabidopsis. The Plant Cell Online *20,* 2860-2875.

United States Department of Agriculture, National Agricultural Statistics Service. (2011). Acreage. Retrieved September 1, 2011, from [http://usda01.library.cornell.edu/usda/current/Acre/Acre-06-30-2011.pdf]

Vanneste, S., and Friml, J. (2009). Auxin: A Trigger for Change in Plant Development. Cell *136,* 1005-1016.

Vollbrecht, E., and Schmidt, R. (2009). Development of the Inflorescences. In Handbook of Maize: It's Biology, Bennetzen, Jeff L., and Hake, Sarah C. eds., (New York, New York: Springer) pp. 13-40.

Walsh, J., and Freeling, M. (1999). The *liguleless2* gene of maize functions during the transition from the vegetative to the reproductive shoot apex. Plant J. *19,* 489-495.

Whipple, C.J., Ciceri, P., Padilla, C.M., Ambrose, B.A., Bandong, S.L., and Schmidt, R.J. (2004). Conservation of B-class floral homeotic gene function between maize and Arabidopsis. Development *131,* 6083-6091.

Wu, X., and McSteen, P. (2007). The role of auxin transport during inflorescence development in maize (Zea mays, Poaceae). Am. J. of Bot. *94,* 1745-1755.